HHS Public Access

Author manuscript

Dev Cell. Author manuscript; available in PMC 2021 June 08.

Published in final edited form as:

Dev Cell. 2020 June 08; 53(5): 577–588.e7. doi:10.1016/j.devcel.2020.05.009.

Long-range optogenetic control of axon guidance overcomes developmental boundaries and defects

James M. Harris[1,2,3], **Andy Yu-Der Wang**[1,4], **Jonathan Boulanger-Weill**[5], **Cristina Santoriello**[1,7], **Stephan Foianini**[5], **Jeff W. Lichtman**[5,6], **Leonard I. Zon**[1,7], **Paola Arlotta**[1,3,*]

[1]Department of Stem Cell and Regenerative Biology, Harvard University, Cambridge, Massachusetts 02138, USA.

[2]Harvard-MIT Division of Health Sciences and Technology, Harvard Medical School, Boston, MA 02115, USA.

[3]Stanley Center for Psychiatric Research, Broad Institute of MIT and Harvard, Cambridge, MA 02138, USA.

[4]Current Address: Tufts University School of Medicine, Boston, MA 02115, USA.

[5]Department of Molecular and Cellular Biology, Harvard University, Cambridge, Massachusetts 02138, USA.

[6]Center for Brain Science, Harvard University, Cambridge, Massachusetts 02138, USA.

[7]Stem Cell Program and Division of Hematology/Oncology, Children's Hospital and Dana Farber Cancer Institute, Howard Hughes Medical Institute, Harvard Medical School, Harvard Stem Cell Institute, Stem Cell and Regenerative Biology Department, Harvard University, Boston, MA 02115, USA.

Abstract

Axons connect neurons together, establishing the wiring architecture of neuronal networks. Axonal connectivity is largely built during embryonic development through highly constrained processes of axon guidance, which have been extensively studied. However, the inability to control axon guidance, and thus neuronal network architecture, has limited investigation of how axonal connections influence subsequent development and functionality of neuronal networks. Here, we use zebrafish motor neurons expressing a photoactivatable Rac1 to co-opt endogenous growth

*Lead contact. Correspondence: Paola_Arlotta@harvard.edu.

Author Contributions: JH and PA conceived and designed the experiments and wrote the manuscript. JH performed the majority of the experiments. AW assisted in performing and analyzing optogenetic stimulation experiments and cloning of DNA constructs. CS and LIZ helped to generate transgenic constructs and to perform transgenesis injections. JBW and SF performed EM experiments under the supervision of JWL. PA supervised all aspects of the project.

Declaration of Interests: L.I.Z. is a founder and stockholder of Fate Therapeutics, Scholar Rock, Amagma Therapeutics, and CAMP4 Therapeutics. He is a consultant for Celularity and Cellarity. Consulting arrangements for P.A. are not relevant or in conflict of interest to the current work. A patent application is pending based on this work (applicants: President and Fellows of Harvard College; inventors: P.A. and J.H.; status: pending; aspect covered: methods and apparatus for optogenetic control of neurite growth). All other authors declare no competing interests.

cone guidance machinery to precisely and noninvasively direct axon growth using light. Axons can be guided over large distances, within complex environments of live organisms, overriding competing endogenous signals and redirecting axons across potent repulsive barriers to construct novel circuitry. Notably, genetic axon guidance defects can be rescued, restoring functional connectivity. These data demonstrate that intrinsic growth cone guidance machinery can be co-opted to non-invasively build new connectivity, allowing investigation of neural network dynamics in intact living organisms.

Graphical Abstract

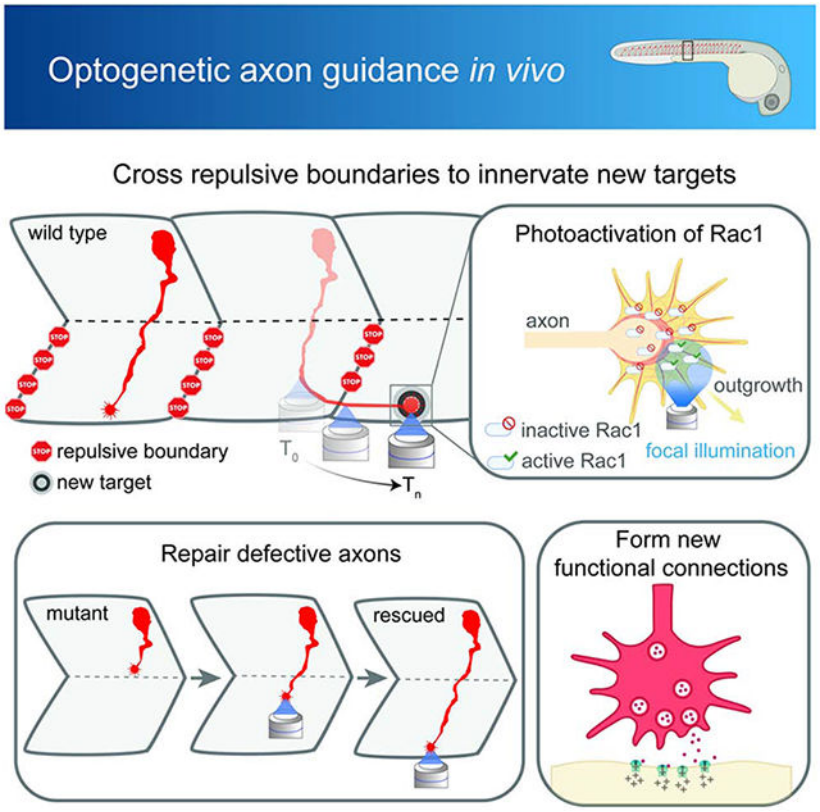

eTOC Blurb

Axons define the long-range connectivity of the nervous system. Using an optogenetic approach, Harris et al. direct axonal growth with light to engineer axonal architectures precisely and non-invasively. Axons can be guided across repulsive developmental barriers to create novel circuitry and functional connectivity can be restored to defective circuits.

Keywords

axon guidance; optogenetics; tissue engineering; neurons; embryonic development; nerve regeneration; axons; zebrafish; rac GTP-binding proteins; neuronal outgrowth

---

Axonal connections define how information flows through neuronal networks. As the nervous system develops, axonal innervation allows for the exchange of molecular and

electrophysiological signals between projecting axons and their target tissues, with axonal input playing a key role in shaping the information processing functions of downstream neuronal networks. One of the most compelling demonstrations for the validity of this neurodevelopmental principle is the fact that sensory areas of the mammalian cerebral cortex switch to processing information of alternative sensory modalities (i.e., visual instead of auditory) when they receive re-routed afferent axonal connectivity from a different sensory organ (Pallas, et al., 1999; Sur, et al., 1999; Pallas and Sur, 1993; Pallas, et al., 1990). Additionally, axonal input plays a significant role in shaping postsynaptic neuronal identity by influencing key cellular properties including neurotransmitter selection, dendritic architecture, gene expression, and electrophysiological features (Dehorter, et al., 2015; De Marco Garcia, et al., 2011). Conversely, retrograde signals from target tissue can shape neurotransmitter expression profiles (Russ and Kaltschmidt, 2014; Kou, et al., 1995) and cell body positioning (Haase, et al., 2002; Lin, et al., 1998) of the projecting neurons. How the molecular and electrophysiological interaction of axons and their targets shape their mutually defined identities and processing functions remains largely unexplored. To pursue these foundational questions, experimental approaches to precisely and noninvasively sculpt axonal connections within the intact organism are required.

During development, the general architecture of neuronal networks is established in a complex, highly reproducible process of axon extension and guidance that allows axons to reliably find their appropriate targets (Tessier-Lavigne, 2002). Great progress has been made in understanding the molecular events in the growth cone, a specialized structure at the leading tip of the axon, that direct outgrowth in appropriate directions during development (Dickson, 2002; Tessier-Lavigne and Goodman, 1996). This knowledge now offers the opportunity to manipulate the endogenous axon guidance machinery to construct novel neuronal circuit architectures and repair defective or injured circuits. If such approaches could be successfully applied within the intact organism, they would enable directed experimental manipulation of circuit wiring, a prerequisite for understanding the rules that wire neuronal networks and define their properties *in vivo*.

Previous work has demonstrated that changes to the molecular composition of the microenvironment in which axons grow can influence their growth trajectories, by ectopically providing guidance factors and permissive environments *in vitro* (Wheeler and Brewer, 2010; Lohof, et al., 1992; Walter, et al., 1987) and *in vivo* (Piantino, et al., 2006; Schnell, et al., 1994; David and Aguayo, 1981; Richardson, et al., 1980). Since these methods rely on the construction of predefined environments to extrinsically influence axonal growth, by definition they lack spatial and temporal flexibility and precision, and require invasive procedures for *in vivo* application. Precise, non-invasive control of the intrinsic axon guidance machinery within the growth cone of individual axons would provide unprecedented capacity and flexibility to direct novel connectivity.

Pioneering optogenetic tools have been used to control intracellular physiology using non-invasive light stimuli that allow subcellular precision (Endo, et al., 2016; Ryu, et al., 2010; Airan, et al., 2009; Wu, et al., 2009; Yazawa, et al., 2009; Zhao, et al., 2008; Boyden, et al., 2005; Kim, et al., 2005; Nagel, et al., 2005). Here, we introduce the use of a photoactivatable Rac1 (PA-Rac1) protein (Hayashi-Takagi, et al., 2015; Yoo, et al., 2010;

Wu, et al., 2009) to manipulate axonal guidance in single axons, to determine whether long-distance axonal connectivity could be redirected. Endogenous Rac1 plays an evolutionarily conserved role in axon guidance by translating positional information from extracellular signaling molecules into appropriate intracellular cytoskeletal responses in the growth cone, resulting in precise steering decisions during axon guidance (Hua, et al., 2015b ; Hall and Lalli, 2010; Ng, et al., 2002). We therefore investigated whether optogenetic control of Rac1 activation could co-opt its intrinsic guidance role. Strikingly, we found that light-induced activation of PA-Rac1 can non-invasively and precisely control axonal guidance in the complex environment of the intact organism, effectively outcompeting endogenous repulsive axon guidance barriers and rescuing genetic axon guidance defects. Most importantly, re-routed axons are capable of making active synapses to establish functional connectivity. This approach unlocks future avenues for engineering axonal connectivity to create novel circuits in real time, within intact, living organisms.

Results

Optogenetic stimulation of PA-Rac1 resulted in directed axonal growth of cultured zebrafish spinal motor neuron axons

In order to investigate whether axon guidance could be controlled by light activation of PA-Rac1, we used spinal motor neurons of the developing zebrafish as a model system. Zebrafish embryos are optically transparent, develop rapidly, and have highly stereotyped programs of spinal motor axon guidance (Beattie, 2000). To express PA-Rac1 specifically in spinal motor neurons, we generated transgenic zebrafish that expressed an optimized PA-Rac1 fused with the mCherry fluorescent reporter under a tissue-specific *mnx1* minimal enhancer (Zelenchuk and Bruses, 2011) and a *β-globin* minimal promoter (Figure 1A). Expression of *PA-Rac1* RNA in spinal motor neurons of transgenic fish was approximately two-fold higher than the endogenous *rac1* genes (*rac1a* and *rac1b*) at 24 hours post fertilization (hpf) (Figure S1A,B), indicating robust expression of the exogenous construct. Nonetheless, given that the PA-Rac1 protein is only active upon illumination and that illumination was restricted to a small portion of the growth cone, it is likely that optogenetically driven Rac1 activity remained within the physiologic range of overall cellular Rac1 activity.

To determine if optogenetic activation of Rac1 could co-opt the endogenous axon guidance machinery in the growth cone, we first used a 2D *in vitro* culture of spinal motor neurons. To clearly identify mCherry-positive spinal motor neurons, we cultured sparse monolayers of dissociated *Tg(mnx1:mCherry-PA-Rac1);mitfa*$^{w2/w2}$*;mpv17*$^{a9/a9}$ zebrafish tails collected at 18hpf, a time when motor neurons have differentiated and expressed PA-Rac1, but before they have completed axonal pathfinding. mCherry-expressing neurons with projecting axons were visually identified, and the growth cone was asymmetrically illuminated with 458nm light in a small region of interest using a Zeiss 880 confocal microscope (see also Methods; Figure 1A). Within 3 to 5 minutes from the start of illumination, growth cones responded by projecting membrane extensions in the direction of the illumination, and by 10 to 20 minutes most axons had visibly extended in the direction of the light stimulus (Figure 1B; Movie S1). The region of stimulation was progressively advanced to guide the growth of each axon

perpendicular to its original trajectory (n=5 axons from separate cultures of independent fish, average illumination time of 83.2 minutes). We compared the directed growth obtained by 458nm illumination of PA-Rac1^{+} axons to the growth of both unilluminated axons and 458nm-illuminated axons from *Tg(mnx1:mCherry-PI-Rac1);mitfa$^{w2/w2}$;mpv17$^{a9/a9}$* fish, which carry a mutated version of PA-Rac1 that renders this construct photo-insensitive (PI-Rac1). We found that light-stimulated PA-Rac1^{+} axons deviated from their initial trajectories at much greater angles compared to unilluminated controls and light-stimulated PI-Rac1^{+} axons (mean deviation angle ± 95% confidence interval (CI): 19.8° ± 20.9°, 25.3° ± 16.0 °, and 99.2° ± 13.8° in unilluminated, PI-Rac1, and PA-Rac1 axons, respectively; Figure 1C). In addition, stimulated growth cones extended axons over greater distances during the trial period (mean distance +/− 95% CI: 3.3 ± 6.1μm, 1.8 ± 3.4μm, 15.4 ± 6.0μm in unilluminated, PI-Rac1, and PA-Rac1 axons, respectively), resulting in faster rates of growth (mean growth rate ± 95% CI: 2.1 ± 4.0 μm/hr, 2.0 ± 3.6μm/hr, and 11.4 ± 5.2μm/hr in unilluminated, PI-Rac1, and PA-Rac1 axons, respectively; Figure 1B,C and Movie S1).

To further control for possible physical effects of laser illumination, we exposed PA-Rac1^{+} growth cones to 514nm light, outside of the spectrum of PA-Rac1 activation followed immediately by exposure to 458nm light, within the spectrum of PA-Rac1 activation. As expected, exposure to 458nm light, but not 514nm light, induced axonal extension in the direction of illumination (Figure S1C,D). To assess if illumination of PA-Rac1^{+} neurons activated Rac1 signaling, we performed immunohistochemistry for autophosphorylated Pak1, which is a major downstream signaling target of Rac1. We saw increased autophosphorylation of Pak1 within a region of illumination compared with the rest of the cell (Figure S1E). These results demonstrate that light activation of PA-Rac1 in growth cones allows targeted, directional control over intrinsic axonal extension programs.

Optogenetic stimulation of PA-Rac1 directed zebrafish CaP axon growth across repulsive somitic boundaries into neighboring somitic musculature

While PA-Rac1 stimulation guided axonal growth in sparse neuronal cultures, *in vivo* applications present additional challenges for engineering axon guidance, including competition from endogenous axonal guidance signals, complex 3D tissue environments, and repulsive molecular and physical barriers. To test if optogenetic axon guidance could overcome these obstacles, we used intact embryonic zebrafish as an *in vivo* model of directed axon growth.

Within each somitic unit of the developing zebrafish, three bilaterally symmetric pairs of primary spinal motor neurons innervate nonoverlapping regions of the animal's somitic musculature (Beattie, 2000; Eisen, et al., 1986) (Figure 2A). Of these neurons, only the caudal primary (CaP) spinal motor neuron extends an axon into the ventral myotome, in a stereotyped path running between the vertical myosepta that separate neighboring somitic myotomes (Beattie, 2000; Eisen, et al., 1986) (Figure 2A). In healthy animals, the path of CaP axons never deviates from this well-defined trajectory (Beattie, 2000; Myers, et al., 1986). This strict pathfinding program is imposed via molecular instructions from several sources within the somite, including repulsive Sema3Ab expressed in the posterior somitic compartment and at the vertical myoseptal boundaries of the somites (Roos, et al., 1999),

repulsive chondroitin sulfate proteoglycans (CPSGs) at vertical myoseptal boundaries (Bernhardt, et al., 1998), and initially attractive and subsequently repulsive Sema5a in the anterior portion of the ventral somite (Hilario, et al., 2009).

Given that Rac1 molecularly links the transduction of a variety of extracellular signals to the cytoskeletal machinery that directs axon growth (Hua, et al., 2015b ; Hall and Lalli, 2010; Ng, et al., 2002), we reasoned that manipulation of Rac1 activity might allow us to override these endogenous axonal guidance signals to drive axonal growth in new directions, within the intact organism. To test this possibility, *Tg(mnx1:mCherry-PA-Rac1);mitfa*$^{w2/w2}$*;mpv17*$^{a9/a9}$ zebrafish were illuminated with 458nm light in a region of interest focused on the leading edge of the CaP growth cone, beginning between 23 and 25hpf, a time when only the CaP axon is extending into the ventral myotome. The region of illumination was periodically updated to attempt to deviate the growing axon in either the rostral or caudal directions over the course of 4 to 5 hours (Figure 2A). Strikingly, we found that in the majority of stimulated axons, growth was deflected in the direction of light application (n=17 axons/23 stimulated, one axon per fish; Figure 2B-E).

As the region of stimulation was updated, 3 of the 23 illuminated axons grew in the direction of light stimulation within their native somite and 14 of the 23 illuminated axons could be guided up to and eventually across the repulsive somitic boundary, extending into the neighboring somitic musculature (Figure 2B-D), despite the presence of strong opposing endogenous signals at this boundary (Roos, et al., 1999; Bernhardt, et al., 1998). We found that axons could be guided across both rostral (Figure 2B,C; Movie S2A) and caudal somitic boundaries (Movie S2B). In contrast, unstimulated neighboring axons never crossed the somitic boundary (n=57 axons, Figure 2E). Stimulated axons grew longer distances than unstimulated ones over the trial period, resulting in faster rates of growth (Figure 2E), a finding that confirms our measurements *in vitro*. In initial experiments, we noted that the direction of axonal growth could be dynamically altered over the course of stimulation, as for the cultured neurons discussed earlier. Furthermore, in two instances, it appeared that the optogenetically guided axons could be induced to grow out of the myotome altogether, continuing their extension ventrally (Figure S2A), while all unstimulated axons remained within the musculature. To investigate these events in greater detail, we performed serial EM reconstructions of one such deviated axon, which confirmed that it grew past the edge of the myotome, extending ventrally to the kidney duct (Figure S2B-F). Interestingly, the EM reconstruction suggests that migratory cells, possibly neural crest or sclerotomal cells, which normally migrate along the same path as the extending CaP axon (Melancon, et al., 1997), also aberrantly accompanied the extending axon to its ectopic target in the kidney (Figure S2E,F).

In these experimental paradigms, optical activation of PA-Rac1 allowed us to direct axonal growth across somitic boundaries, such that the deviated axons became juxtaposed with the myotome of the neighboring somite, a target these axons do not typically innervate. To test whether new connectivity could be established between the directed, aberrant axons and their new ectopic targets, we looked for evidence of synapse formation. First, we deviated CaP axons across the rostral somitic boundary and into the neighboring somite as described above (Figure 2A). To allow time for synapse formation, embryos were grown for an

additional 1.5 hours past the end of stimulation before fixation. Immunohistochemical detection of mCherry-expressing CaP axons confirmed that the stimulated axon did indeed cross the somitic boundary (Figure 3A), passing laterally to the CaP axon of the neighboring somite (Figure 3B,C; Movie S3). Within the target somitic myotome, both the deviated axon and the axon native to the invaded somite (control) exhibited significant colocalization of the presynaptic marker synaptic vesicle protein 2 (SV2) with postsynaptic acetylcholine receptors (αBT), as quantified by volumetric signal correlation (mean Pearson's correlation coefficient ± 95% confidence interval 0.347 ± 0.086 95%, n=3 fish, Costes p-value >0.95; Figure 3D,E), suggesting the presence of ectopic neuromuscular junctions between the deviated axon and the musculature of the neighboring, invaded somite.

Optogenetic stimulation of *plod3*$^{-/-}$ zebrafish CaP neurons rescued their axon guidance defect, allowing functional synaptic connectivity with the ventral myotome.

In our experiments, optogenetic activation of Rac1 was sufficient to control the guidance of otherwise normally-developing CaP motor neurons in the context of a wild-type tissue environment. To test whether optogenetically directed axonal growth could also rescue CaP axon guidance defects in a pathological environment, we employed a zebrafish mutant in which CaP axon pathfinding and connectivity are disrupted. Specifically, we used *plod3*^{tv205a} mutant zebrafish (which we refer to as *plod3*$^{-}$), that carry a loss-of-function point mutation in the lh3 glycosyltransferase *plod3* (Schneider and Granato, 2006). Animals homozygous for this mutation have disrupted myotomal type XVIII collagen, and consequently display premature cessation of CaP motor neuron growth cone pathfinding at or before the horizontal myoseptum, with associated failure to extend appropriately into the ventral myotome (Figure 4A-D) (Schneider and Granato, 2006; Zeller and Granato, 1999; Granato, et al., 1996).

We generated transgenic *plod3*$^{-/-}$ mutant embryos expressing PA-Rac1 in spinal motor neurons (see also Methods) and attempted to rescue axon guidance defects in the CaP neurons using optogenetic stimulation. We initiated light guidance in mutant growth cones at 28hpf, a point at which CaP axons of heterozygote *plod3*$^{+/-}$ animals have projected well beyond the horizontal myoseptum (Figure 4A), but growth cones of *plod3*$^{-/-}$ fish have stalled at this boundary. We found that the illuminated axons grew significantly farther past the horizontal myosepta compared with their neighboring, unilluminated axons ($p<0.001$, FDR adjusted, difference of least square means from mixed linear model), and extended distances that were not significantly different from wildtype fish (mean distance from CaP axon tip to the horizontal myoseptum ± 95% confidence interval: 0.2 ± 2.5μm, 63.6 ± 9.2μm, and 44.9 ± 16.5μm in *plod3*$^{-/-}$ fish, *plod3*$^{+/-}$ fish, and optogenetically rescued *plod3*$^{-/-}$ fish respectively, n=8 axons, one axon per fish; Figure 4B-D; Movie S4). Furthermore, immunohistochemical detection of pre- and post-synaptic proteins indicated that the rescued CaP axons could form synaptic connections with the surrounding myotome (Figure 4E).

In order to determine whether functional synapses were formed between the optogenetically-rescued *plod3*$^{-/-}$ CaP axons and the myotome, we generated *plod3*$^{-/-}$ zebrafish that expressed both PA-Rac1 and ReaChR, a red-shifted channelrhodopsin (Lin, et al., 2013) in

spinal motor neurons (Figure 5A). First, we rescued the axonal guidance defect in *plod3*$^{-/-}$ mutants, growing axons into the ventral myotome as described above (Figure 5A,B; Movie S5). Following rescue, we induced neural activity in these neurons by stimulating the ReaChR channelrhodopsin using 594nm and 633nm light. ReaChR stimulation produced muscle contractions that in >85% of cases were specifically restricted to the ventral myofibrils innervated by the redirected axon (15/17 contractions, Figure 5D), as assessed using motion tracking with particle image velocimetry analysis (see also Methods) (Figure 5E; Movies S6,7). To control for axonal depolarization outside of the ventral myotome and the physical effects of light exposure, we illuminated neighboring un-rescued axons with the same wavelengths of light (549nm and 633nm) or illuminated rescued axons with 405nm and 440nm light, outside the spectrum of ReaChR activation. We found that ReaChR activation of rescued axons resulted in significantly more contractions of the ventral myotome in the targeted somite than either control condition (n=3 fish, 5 trials per condition in each fish, Figure 5F; Movies S6). We performed immunohistochemistry for synaptic markers (SV2 and αBT) on the same experimental animals after conclusion of the stimulation experiments. We observed that presynaptic SV2 (in the rescued *plod3*$^{-/-}$ CaP axons) and postsynaptic αBT (in the ventral myofibrils) were significantly colocalized, indicating that the recovery of synaptic function observed using optogenetic stimulation correlates with molecular evidence of synapse formation (mean Pearson's correlation coefficient ± 95% confidence interval 0.367 ± 0.105, n=3 fish, Costes p-value>0.95; Figure 5C). Thus, PA-Rac1-mediated axonal rescue resulted in formation of functional synaptic connectivity between the rescued axons and their new ventral myofibril targets, demonstrating that PA-Rac1 activation can be used to rescue defective axon guidance within the intact developing organism despite a pathologic environment that lacks type XVIII collagen, a necessary myotomal guidance signal. All together, these results show that PA-Rac1 provides a powerful means to direct axonal growth at the level of individual growth cones, irrespective of endogenous repulsive barriers or defective pathfinding signaling to create functional circuitry.

Discussion

The ability to manipulate axonal growth and guidance in living organisms would offer an opportunity for experimental investigation of fundamental neurodevelopmental questions regarding the relationship between axons and their targets and how network architecture shapes the development and function of the nervous system.

New approaches are needed to allow precise and noninvasive sculpting of axonal connections in the intact organism. Manipulating axonal growth trajectories in living organisms is particularly challenging, since growth cones are subjected to complex physical and molecular environments that have evolved to ensure axons adopt specific morphologies and only connect to stereotyped targets (Dickson, 2002; Tessier-Lavigne and Goodman, 1996). The ability to direct axons to new targets across these powerful endogenous repulsive barriers is necessary to wire novel circuitry *in vivo*, where a diversity of axon guidance signals would otherwise impede directed re-wiring.

In addition to guidance during development, axons can also encounter pathfinding barriers that impede regeneration following injury. Here we showed that CaP axon growth could be directed across vertical myoseptal boundaries, which are typically never crossed (Beattie, 2000; Myers, et al., 1986) due to potent molecular deterrents including chondroitin sulfate proteoglycans (CSPGs) and semaphorins (Roos, et al., 1999; Bernhardt, et al., 1998). Interestingly, a number of these same inhibitory molecules have homologues in glial scars, which form following injury in the mammalian CNS (Siebert, et al., 2014; Pasterkamp, et al., 1999). These scars become impenetrable barriers, and are a major obstacle for subsequent axonal regeneration (Yiu and He, 2006). The ability to overcome such molecular barriers in the zebrafish opens new doors to investigation of similar non-invasive guidance approaches to aid regeneration of mammalian axons.

In order to functionally repair and rewire circuitry, active synaptic connectivity must be established between the redirected axon and its new target. Optogenetic activation of PA-Rac1 in CaP neurons could not only overcome the axon guidance defects associated with pathological loss of *plod3* activity, but also resulted in the formation of new functional synapses, capable of mediating ventral myofibril contraction following optogenetic depolarization of the rescued axons. These results serve as a proof-of-principle for the application of this approach to wire novel circuitry to investigate the role of new connectivity on target development and function.

In addition to enabling future investigation into the development, function, and possibly regeneration of neuronal networks, our experimental paradigm suggests an intriguing application to the engineering of neural networks *in vitro*. Human induced pluripotent and embryonic stem cells can be differentiated into neurons in a variety of culture configurations ranging from monolayers to 3D brain organoids (Velasco, et al., 2019; Quadrato and Arlotta, 2017). Endogenous patterns of connectivity, however, are difficult to attain within these model systems, setting practical limits on *in vitro* studies of human circuit formation and functionality. Although here we manipulated single growth cones, the use of light as a stimulus allows enormous flexibility in delivering patterned stimulation to these *in vitro* models. For instance, digital micromirror devices (DMDs) provide a scalable, parallel method for generating complex patterns of light (de Beco, et al., 2018; Hakim, et al., 2018; Jung, et al., 2017; Brinks, et al., 2016; Avants, et al., 2015; Sakai, et al., 2013). Future work could combine these devices with the optogenetic axon guidance approach demonstrated here, to guide many axons simultaneously and create precise, realistic, and reproducible axonal architectures in complex three-dimensional *in vitro* models, such as brain organoids.

Beyond its potential for powerful applications in the nervous system, this work also serves as an example of how optogenetic control of cellular morphology can reshape development to engineer novel tissue architectures, an approach that may carry particular value for regenerative biology and tissue engineering across a variety of tissue types.

STAR Methods:

RESOURCE AVAILABILITY

Lead Contact—Further information and requests for resources and reagents should be directed to and will be fulfilled by the Lead Contact, Paola Arlotta (Paola_Arlotta@harvard.edu).

Materials Availability—Transgenesis constructs will be available from Addgene upon publication.

Data and Code Availability—The datasets and code generated during this study are available on github (https://github.com/jharris9/optogenetic_axon_guidance_analysis) and from the corresponding author upon request.

EXPERIMENTAL MODEL AND SUBJECT DETAILS

Zebrafish—All zebrafish (*Danio rerio*) lines were grown under standard conditions (16:8 hour light dark cycle at 28.5°C) approved by the Harvard Institutional Animal Care and Use Committee (IACUC). Transgenic lines were derived from two initial strains: *mitfa*^{w2}*;mpv17*^{a9} transparent fish (ZIRC ZL1714)(White, et al., 2008), or *plod3*^{tv205a} mutant fish that have disrupted spinal motor neuron axon guidance in homozygotes (European Zebrafish Resource Center #941) (Schneider and Granato, 2006; Granato, et al., 1996). From these two initial lines, transgenic animals were created to express an optimized photoactivatable Rac1 (PA-Rac1) (Hayashi-Takagi, et al., 2015; Lungu, et al., 2012), a light insensitive mutant Rac1 (PI-Rac1) (Wu, et al., 2009), or a red-shifted channelrhodopsin (ReaChR) (Lin, et al., 2013), in spinal motor neurons. Three stable transgenic lines were created: *Tg(mnx1:mCherry-PA-Rac1);mitfa*^{w2}*;mpv17*^{a9}*, Tg(mnx1:mCherry-PI-Rac1);mitfa*^{w2}*;mpv17*^{a9}, and *Tg(mnx1:mCherry-PA-Rac1);plod3*^{tv205a}. Embryos were visually screened at 48hpf for mCherry expression in spinal motor neurons using a Zeiss fluorescent dissecting microscope; positive fish were grown to adulthood and outcrossed to identify founders with germline transmission. Male and female embryos from incrosses of founders and progeny were used for subsequent experiments between 18 and 32hpf. All control animals were clutchmates, or age-matched if clutchmates were unavailable.

In addition to generating stable lines, transient transgenesis was performed to create *Tg(mnx1:ReaChR-citrine);Tg(mnx1:mCherry-PA-Rac1);plod3*^{tv205atv205a} fish, by injecting *Tg(mnx1:mCherry-PA-Rac1);plod3*^{tv205atv205a} embryos with the *pDestTol2CG2-mnx1:ReaChR-citrine* transgenesis construct. To determine experimental candidates, transgenic fish were screened for strong expression of mCherry-PA-Rac1, mCherry-PI-Rac1, or ReaChR-citrine transgenes by visualization of their respective fluorophores in CaP motor neurons.

Primary zebrafish motor neuron cultures—Primary zebrafish motor neurons were cultured from pooled 18hpf male and female *Tg(mnx1:mCherry-PA-Rac1);mitfa*$^{w2/w2}$*;mpv17*$^{a9/a9}$ and *Tg(mnx1:mCherry-PI-Rac1);mitfa*$^{w2/w2}$*;mpv17*$^{a9/a9}$ fish

at room temperature in Leibovitz's L-15 media (Thermo Fischer 21083027) supplemented with 2% fetal bovine serum and 100U/mL penicillin/streptomycin.

METHOD DETAILS

Plod3^{tv205a} genotyping—DNA was extracted from tail clippings of adult zebrafish using the DNAeasy Blood and Tissue kit (Qiagen 69504). *Plod3 ^{tv205a}* fish were genotyped using a Custom TaqMan SNP genotyping assay (Thermo Fisher 4332077, Assay ID ANXGU9F) with an Applied Biosystems 7900HT RT-PCR machine, according to the manufacturer's instructions.

Cloning of transgenesis constructs—To generate transgenic zebrafish lines, three transgenesis constructs were created: *pDestTol2CG2-mnx1:mCherry-PA-Rac1*, *pDestTol2CG2-mnx1:mCherry-PI-Rac1*, and *pDestTol2CG2-mnx1:ReaChR-citrine*. The Multisite Gateway technology (Invitrogen) and the Tol2 Kit (Kwan, et al., 2007) were used to generate *pDestTol2CG2-mnx1:mCherry-PA-Rac1*, according to the manufacturer's instructions. Three entry vectors were used: a 5' entry vector (*p5E*), a middle entry vector (*pME*), and a 3' entry vector (*p3E*). The *p5E* entry vector contained three tandem repeats of a 125bp *mnx1* enhancer to drive transgene expression in zebrafish spinal motor neurons, and was constructed as described previously (Zelenchuk and Bruses, 2011). Briefly, 3 copies of the 125bp *mnx1* enhancer were PCR amplified from a 3kb portion of the *mnx1* promoter with 3 sets of primers with unique restriction sites (primers and restriction enzymes listed in Table S1). PCR products were digested, gel purified, and sequentially cloned into the *p5E* vector using the pENTR 5'-TOPO TA Cloning kit (Invitrogen K59120, Tol2Kit plasmid #228)(Kwan, et al., 2007). The *pME* vector contained the mouse *β-globin* minimal promoter (Tamplin, et al., 2011) and *mCherry-PA-Rac1* optimized to reduce background activity in the absence of light stimulation by introducing the previously described L514K and L531E mutations in the J-α helix (Hayashi-Takagi, et al., 2015; Lungu, et al., 2012). These mutations were introduced into the *pTriEx-mCherry-PA-Rac1* plasmid (a gift from Klaus Hahn; Addgene plasmid #22027) (Wu, et al., 2009) using the Q5 site-directed mutagenesis kit according to the manufacturer's instructions (NEB E0554S, primers listed in Table S1). The L514K mutation altered two bases and required two sequential rounds of site directed mutagenesis, one for each base. This optimized *PA-Rac1* was PCR amplified, gel purified, and TOPO cloned into the *pENTR* vector (Invitrogen K240020) using primers listed in Table S1. The mouse *β-globin* minimal promoter (Tamplin, et al., 2011) was PCR amplified and inserted upstream of optimized *mCherry-PA-Rac1* in the *pME-mCherry-PA-Rac1* vector linearized with NotI using Gibson Assembly (NEB E5510S, primers listed in Table S1) to allow robust gene expression. The *p3E* vector contained an SV40 poly-A signal (Tol2Kit plasmid #302)(Kwan, et al., 2007). The *p5E-3x125bp-mnx1*, *pME-B-globin-mCherry-PA-Rac1*, and *p3E-SV40-poly-A* entry vectors were recombined with the *pDestTol2CG2* destination vector (Tol2Kit plasmid #395)(Kwan, et al., 2007) using LR Clonase II Plus according to the manufacturer's instructions (Invitrogen 12538200) to produce the final transgenesis constructs (Figure 1A).

To generate the *pDestTol2CG2-mnx1:ReaChR-citrine* plasmid, a *pME* vector containing the *β-globin* minimal promoter and *ReaChR-citrine* was constructed by swapping *mCherry-PA-*

Rac1 for *ReaChR-citrine* in the *pME-B-globin-mCherry-PA-Rac1* vector. Briefly, *mCherry-PA-Rac1* was removed from *pME-B-globin-mCherry-PA-Rac1* using BssHII and HpaI digestion and the backbone fragment was gel purified. A *ReaChR-citrine* PCR product amplified from Addgene plasmid #50956 (a gift from Roger Tsien) (Lin et al., 2013) and a PCR amplified fragment of the backbone lost in the restriction reaction were gel purified and inserted using the NEBuilder HiFi DNA Assembly kit according to the manufacturer's instructions (NEB E2621, primers listed in Table S1). The final transgenesis construct was generated via recombination as described above.

To generate the light insensitive *pDestTol2CG2-mnx1:mCherry-PI-Rac1* transgenesis construct, L514K and L531E mutations were introduced into the *pTriEx-mCherry-PA-Rac1-C450A* plasmid (a gift from Klaus Hahn; Addgene plasmid #81031), which harbors a single amino acid substitution rendering PA-Rac1 insensitive to light (Wu, et al., 2009), and which we refer to as PI-Rac1. Thus, PA-Rac1 and PI-Rac1 were identical except for the C450A mutation rendering PI-Rac1 insensitive to light. The *pDestTol2CG2-mnx1:mCherry-PA-Rac1* and *pTriEx-mCherry-PA-Rac1-C450A* plasmids were digested with AgeI and BbvCI and the *PI-Rac1* fragment and the destination vector backbone were gel purified and ligated together using Quick T4 DNA ligase (NEB M2200S) to create the final transgenesis construct. All cloning reactions were sequence verified.

Zebrafish transgenesis—Transgenic lines were derived by injecting *mitfa*$^{w2/w2}$;*mpv17*$^{a9/a9}$ or *plod3*$^{tv205a/+}$ embryos at the one-cell stage with 1nL of 25ng/uL of *pDestTol2CG2-mnx1:mCherry-PA-Rac1*, *pDestTol2CG2-mnx1:mCherry-PI-Rac1*, or *pDestTol2CG2-mnx1:ReaChR-citrine* transgenesis constructs along with 35ng/uL Tol2 mRNA. Capped Tol2 mRNA was transcribed *in vitro* using the mMessage mMachine SP6 kit (Ambion AM1340) from a NotI linearized *pCS2FA-transposase* plasmid (Tol2Kit plasmid #396)(Kawakami and Shima, 1999) according to the manufacturer's instructions. Tol2 RNA was purified with the RNAeasy Mini Kit (Qiagen 74104).

Zebrafish embryo dissociation and culture—Nitric-acid etched glass coverslips (25mm No 1.5; neuVitro GG-25-1.5-Pre) were incubated with 100ug/mL poly-D-lysine (VWR 35210) in 100mM borate buffer overnight at room temperature. The following day, coverslips were washed 5x with phosphate buffered saline (PBS), followed by incubation with 5ug/mL of laminin (VWR 354232) in water for one hour at 37°C. Coverslips were then washed twice with sterile water. Randomly selected embryonic zebrafish at 18hpf were dissociated as described previously (Andersen, 2001). Briefly, the outer chorionic surface was sterilized for 5 seconds in 70% ethanol. Embryos were then washed twice and then anesthetized in E3 (5mM NaCl, 0.17mM KCl, 0.33mM $CaCl_2$, 0.33mM $MgSO_4$) with 0.0016% tricaine (MS-222; Sigma-Aldrich E10505) for 10 minutes before manual removal of the chorion. Embryos were washed twice in MMR (100mM NaCl, 2mM KCl, 1mM $MgSO_4$, 2mM $CaCl_2$ and 5mM Na-HEPES, adjusted to pH 7.8 with NaOH) and the skin and head were dissected away. The body was incubated in 100uL of ATV solution (0.6mM EDTA, 5.5mM glucose, 5.4mM KCl, 136.8mM NaCl, 0.05% trypsin, 5.5mM Na_2CO_3) for 10 minutes at 30°C followed by trituration with a 10uL pipette tip 30 times. Culture media (2% fetal bovine serum, 100U/mL penicillin/streptomycin in Liebowitz L-15 media

[Thermo Fischer 21083027]) was then added. A pool of three embryos was plated on each coverslip and incubated at room temperature overnight before stimulation trials.

Imaging and optogenetic stimulation—Whole zebrafish embryos were mounted in 1% low melt agarose (Sigma A6877), while primary neurons grown on coverslips were mounted in Attofluor Cell Chambers (ThermoFischer A-7816) for imaging and stimulation experiments. Live embryos were anesthetized with 0.0016% tricaine (MS-222; Sigma-Aldrich E10505) in E3 solution prior to mounting in 1% low melt agarose in tricaine solution. Transmitted and fluorescent images of embryos and primary motor neurons were collected using a Zeiss 880 LSM confocal microscope with a GaSaP detector using the 20X objective (Plan-Apochromat 20x/0.8 NA M27) focused in the plane of the growth cone during stimulation experiments. These images were used to create time-lapse movies with a custom Jython script using the ImageJ API. For still “snapshots”, an AiryScan detector was used to acquire fluorescent Z-stacks for whole zebrafish embryos or a single Z plane for primary motor neuron cultures. Snapshots were acquired at 4-6 timepoints during PA-Rac1 stimulation experiments and following immunohistochemistry. For *in vitro* Pak1 immunohistochemistry experiments, neurons were imaged using a Plan-Apochromat 63x/1.4 NA oil DIC M27 lens. AiryScan deconvolution was performed on images collected with the AiryScan detector using the AiryScan module in ZEN Black (Zeiss). Maximum intensity projections of Z stacks or three-dimensional representations are shown for whole embryos. 3D rendering of confocal Z-stacks was done using VAST (Berger, et al., 2018).

For both *in vitro* and *in vivo* PA-Rac1 optogenetic stimulation experiments, a 3-10μm diameter circle was raster scanned with 5% laser power of 458nm wavelength light (300-650nW, measured with a ThorLabs PM100D optical power meter) through the 20X objective in a region of interest (ROI) placed asymmetrically on the leading edge of the growth cones in the direction of desired outgrowth. Stimulation and imaging were alternated without delay with each stimulation lasting roughly 2 milliseconds and each stimulation/imaging cycle lasting 1-3 seconds. This cycle was repeated until the axon extended into the ROI, at which point the ROI was manually updated in the direction of desired growth. This process was repeated throughout the duration of the trial (up to 90 minutes for *in vitro* experiments and up to 4 hours for *in vivo* experiments). An identical illumination procedure was followed for *in vitro* control experiments of axons expressing the photo-insensitive Rac1 (PI-Rac1).

To determine the effect of wavelength on axonal outgrowth, the growth cones of cultured zebrafish motor neurons expressing PA-Rac1 were exposed to 514nm light (outside the spectrum of PA-Rac1 activation) for 5 minutes, followed by exposure to 458nm light (within the spectrum of PA-Rac1 activation) within the same region of interest. For assessment of Rac1 signaling activity, PA-Rac1 expressing cultured zebrafish motor neurons were exposed to 458nm light in a region of interest as described above for 5 minutes and then immediately fixed for immunohistochemistry of downstream Pak1 phosphorylation.

For *in vivo* deviation of axons across somite boundaries in *Tg(mnx1:mCherry-PA-Rac1);mitfa*$^{w2/w2}$*;mpv17*$^{a9/a9}$ fish, stimulation was initiated between 23 and 25hpf. For rescue experiments of *Tg(mnx1:mCherry-PA-Rac1);plod3*$^{tv205a/tv205a}$ fish, stimulation was

initiated later at 28hpf to ensure that mutant CaP axons were stalled at the horizontal myoseptum prior to stimulation. All *in vivo* stimulation experiments were replicated in independent fish from distinct clutches on separate days and one neuron was optogenetically manipulated per fish. Candidate neurons for optogenetic stimulation were selected based on appropriate initial axonal morphology and strong transgene expression.

For functional interrogation of synapse formation with ReaChR optogenetic depolarization, mounting agarose was dissected away from the zebrafish embryos following PA-Rac1 mediated optogenetic rescue of *plod3*$^{tv205a/tv205a}$ axons. Embryos were placed in room temperature E3 solution for 1.5 hours to ensure removal of tricaine anesthetic and to allow time for synapses to form. Embryos were then transferred to 4°C E3 solution for 1 minute to anesthetize them before remounting in 1% low melting point agarose in E3. ReaChR optogenetic depolarization trials were performed using a similar illumination strategy by raster scanning a region of interest surrounding the target neuron with 100% laser power of 594nm and 633nm light, within the ReaChR activation spectrum. Stimulation trials tested three conditions: ReaChR activation of the rescued neuron, ReaChR activation of a neighboring neuron whose axonal morphology was not rescued, and illumination of the rescued neuron with 100% laser power 405nm and 440nm light (which are outside of the ReaChR activation spectrum) in the same ROI, to control for light exposure. Each stimulation trial consisted of a time series of 1000 bright field imaging frames acquired at 9.5 Hz as described above, with optogenetic stimulation occurring every 200 frames for 100msec, for a total of 5 stimulations per trial. Five trials were performed per condition (n = 3 fish, each tested for all conditions). All stimulation experiments were performed at room temperature.

FACS purification and digital droplet PCR—Randomly sampled embryonic *Tg(mnx1:mCherry-PA-Rac1);mitfa*$^{w2/w2}$*;mpv17*$^{a9/a9}$ zebrafish were dissociated at 24hpf as described above. This age was chosen for gene expression analysis as it corresponded to the time of initiation of *in vivo* axon guidance experiments. mCherry-expressing spinal motor neurons were FACS-sorted into Trizol LS (Thermo Fisher 10296010) using a MoFlo XDP Cell Sorter (Beckman Coulter ML99030) with Summit 5.4 (Beckman Coulter) data collection software. Total RNA was purified from 10,000 sorted cells according to the Trizol LS manufacturer's instructions. cDNA was synthesized using the iScript Select cDNA synthesis kit (BioRad 1708896) with random primers. Digital droplet PCR was performed to quantify *rac1a*, *rac1b*, and *mCherry* expression in sorted spinal motor neurons using the QX200 Evagreen ddPCR supermix (BioRad 1864033) with a QX200 ddPCR machine (BioRad)(primers in Table S1 (Jacobs, et al., 2018; Rosowski, et al., 2016)). *mCherry* expression was used as a proxy for *PA-Rac1* expression, since they originate from a single transcript.

Immunohistochemistry—For *in vivo* experiments, whole mount immunohistochemistry protocols were adapted from previous methods (Panzer, et al., 2005). To allow time for synapse formation, zebrafish embryos were fixed 1.5 hours following the termination of optogenetic stimulation experiments in 4% paraformaldehyde in PBS overnight at 4°C. Embryos were washed three times for five minutes in PBT (0.1% Tween20 and 1% DMSO

in PBS), heads were removed, and the tails were incubated for 45 minutes in 1mg/mL collagenase (Sigma-Aldrich C9891) in PBS. They were then washed three times in PBT for five minutes, and incubated in blocking solution (2% BSA, 0.5% TritonX in PBS) for several hours. They were then incubated with mouse anti-synaptic vesicle 2 (1:100 DSHB SV2) and rabbit anti-RFP (1:500, Rockland 600-401-379S Lot 35868) primary antibodies in blocking solution overnight at 4°C. Embryo tails were washed 5X with PBT and incubated overnight at 4°C with AlexaFluor 488 conjugated goat anti-mouse (1:750, Invitrogen A11001) and AlexaFluor 546 conjugated goat anti-rabbit (1:750, Invitrogen A11035) secondary antibodies in blocking solution. Alexfluor 647-conjugated α-bungarotoxin (Thermo B35450) was added during the last 45 minutes of secondary antibody incubation. The embryo tails were washed three times in PBT for five minutes each before mounting in 1% low melting point agarose (Sigma A6877) in PBS for confocal imaging.

For *in vitro* experiments, after 5 minutes of PA-Rac1 optogenetic stimulation as described above, cultured zebrafish motor neurons were immediately fixed in 4% paraformaldehyde in PBS overnight at 4°C, washed three times in PBT for five minutes each, and incubated in blocking solution as above. They were then incubated overnight with rabbit anti-Thr423 phospho-PAK1 (1:100, Cell Signaling Technology 2601T) and rat anti-RFP (1:100, ChromoTek 5F8) primary antibody in blocking solution. Coverslips were washed three times in PBT for five minutes each, followed by incubation with AlexaFluor 488-conjugated goat anti-rabbit (1:750, Invitrogen A11008) and AlexaFluor 546-conjugated goat anti-rat (1:750, Invitrogen A11081) secondary antibody in blocking solution. Coverslips were washed three times with PBT for five minutes each and mounted with Fluoromount-G (SouthernBiotech 0100-01).

Dissection and tissue preparation for EM—Following induced axon guidance experiments, *Tg(mnx1:mCherry-PA-Rac1);mitfa*$^{w2/w2}$*;mpv17*$^{a9/a9}$ embryos (~30hpf) still under anesthesia were placed in a dissection solution (64 mM NaCl, 2.9 mM KCl, 10 mM HEPES, 10 mM glucose, 164 mM sucrose, 1.2 mM $MgCl_2$, 2.1 mM $CaCl_2$, pH 7.5) (Hildebrand, et al., 2017). Embryos were carefully removed from the agarose and grown for an additional 1.5 hours. The tail was then isolated using sharp scissors (WPI 501778) and immediately transferred to fixative at 4°C (2.5% glutaraldehyde, 2 % PFA in 0.5x cacodylate buffer supplemented with 3.5% mannitol, pH 7.4, Cacodylate buffer: 0.3M sodium cacodylate, 6mM $CaCl_2$, pH7.4). To improve fixation, the tissue was immediately microwaved (Ted Pella, cat. no. 36700, with power controller, steady-temperature water recirculator and cold spot) in the fixative solution at 10°C (<5 min after initial transfer into fixative). The following microwaving sequence was performed: at power level 1 (100 W) for 1 min on, 1 min off, 1 min on; then increased to power level 3 (300 W) and fixed for 20s on, 20s off, 20s on, three times (Tapia, et al., 2012). Fixation was then continued overnight at 4°C in the same solution. The following day, samples were washed in 0.5X cacodylate buffer (3 exchanges, 30 min each at room temperature) and then reduced in freshly made 0.8% (w/v) sodium hydrosulfite in 60% (v/v) 0.1 M sodium bicarbonate, 40% (v/v) 0.1 M sodium carbonate buffer with 3 mM $CaCl_2$ for 20 min at room temperature (Joesch, et al., 2016). This step improves contrast-to-noise ratio between membrane and cytosol. Samples were then washed again in 0.5x cacodylate buffer (3 exchanges, 30 min each at room

temperature) before osmication (2% OsO_4 in 0.5x cacodylate buffer, 4 h at room temperature), and then incubated overnight at 4°C. Samples were then reduced in 2.5% potassium ferrocyanide in 0.5x cacodylate buffer for 4 h at room temperature and then overnight at 4°C. The following day, samples were washed with filtered H_2O (3 exchanges, 30 min each at room temperature) and incubated with 1% (w/v) thiocarbohydrazide (TCH) in H_2O (filtered with a 0.20 μm syringe filter before use) at room temperature to enhance staining (Hua, et al., 2015a). Due to poor dissolution of TCH in water, the solution was heated at 60°C for ~1h with occasional shaking before filtering. Samples were then washed with filtered H_2O (3 exchanges, 30 min each at room temperature) before the second osmication (2% OsO4 in filtered H_2O, 4 h at room temperature) and then washed again (3 exchanges, 30 min each at room temperature). *en bloc* staining was performed using 1% uranyl acetate overnight in filtered water. The OsO^4 solution was sonicated for ~1h and then filtered with a 0.20 μm syringe filter before use. The following day, samples were washed with filtered H_2O (3 exchanges, 30 min each at room temperature) and dehydrated in serial dilutions of ethanol (25%, 50%, 75%, 90%, 100%, 100% for 10min each) followed by propylene oxide (PO) (100%, 100%, 30min each). Infiltration was performed using LX112 epoxy resin with BDMA (21212, Ladd) in serial PO dilutions steps (25% resin/75% PO, 50% resin/50% PO, 75% resin/25% PO, 100% resin, 100% resin, 4h each). Samples were mounted using a mouse brain as support tissue (Hildebrand, et al., 2017) in fresh resin to facilitate cutting. For this, mouse tissue was fixed using standard procedures, pierced using a puncher (EMS 57395) to insert the sample, and stained along with fish samples. The samples with support tissue were then cured for 3 days at 60°C. A rotator was used for all steps. Aqueous solutions were prepared with water passed through a purification system (Arium 611VF, Sartorius Stedim Biotech).

Electron microscopy—The cured blocks were trimmed as previously described (Hildebrand, et al., 2017) and ~30nm sections were automatically collected using a custom tape collection device (ATUM) (Hayworth, et al., 2014) mounted to a commercial ultramicrotome. Sections were collected and post-stained as published (Hildebrand, et al., 2017). Images were acquired using back-scatter detection with a Sigma scanning electron microscope (Carl Zeiss) equipped with the ATLAS software (Fibics). Custom made algorithms were used for non-affine alignment, and volume annotation and segmentation were performed with VAST (Berger, et al., 2018).

QUANTIFICATION AND STATISTICAL ANALYSIS

Analysis of PA-Rac1 axon guidance—For all experiments using transgenic zebrafish, candidate animals were first visually screened for high transgene expression. For *in vitro* optogenetic axon guidance experiments (Figure 1), each replicate represents an axon from a separate culture with cells from independent *Tg(mnx1:mCherry-PA-Rac1);mitfa*$^{w2/w2}$*;mpv17*$^{a9/a9}$ or *Tg(mnx1:mCherry-PI-Rac1);mitfa*$^{w2/w2}$*;mpv17*$^{a9/a9}$ fish. Cultures were randomly assigned to treatment conditions where applicable. Candidate axons were selected based on high expression of mCherry-PA-Rac1 or mCherry-PI-Rac1 and lack of contact of growth cones with any neighboring cells. To quantify *in vitro* optogenetic guidance (Figure 1C), the distance grown by CaP axons over the course of the stimulation experiments and the deviation from their original growth trajectories were measured using

the neurite tracing function of Imaris (Bitplane) and FIJI (ImageJ 2.0.0-rc-69/1.52p) respectively. The distance grown was quantified by taking the difference of the length of the axon before and after the stimulation trial. The speed of growth was calculated by dividing this distance by the time elapsed over the course of the stimulation trial. The angle of axonal trajectory deviation was measured using overlapped images of axons immediately prior to optogenetic stimulation with images of axons following stimulation. An angle of 0° reflected no change in trajectory, while any deviation was considered a positive angle of deflection, since there was no anatomic frame of reference in the monolayer cultures. Measurements were performed on stimulated PA-Rac1 expressing axons, as well as two controls: unstimulated PA-Rac1 expressing neurons and stimulated axons expressing photo-insensitive PI-Rac1. Independent samples Student's T-tests were used to compare each control condition to PA-Rac1 stimulated axons.

For *in vitro* control experiments (Figure S1C,D), candidate cultured *Tg(mnx1:mCherry-PA-Rac1);mitfa*$^{w2/w2}$*;mpv17*$^{a9/a9}$ zebrafish motor neurons were selected as described above and outgrowth was measured in response to different wavelengths of light. Specifically, the area occupied by the growth cone within the region of illumination was measured before and after 5 minutes of exposure first to 514nm light (outside the activation spectrum of PA-Rac1) and then to 5 minutes of 458nm light (which activates PA-Rac1). Since the experimental conditions were applied to the same growth cones sequentially, the responses to different wavelengths were compared with a paired samples Student's T-test.

For optogenetic guidance across somitic boundaries *in vivo* in *Tg(mnx1:mCherry-PA-Rac1);mitfa*$^{w2/w2}$*;mpv17*$^{a9/a9}$ zebrafish (Figures 2,3), candidate axons for optogenetic manipulation were selected based on high transgene expression and having growth cones between the horizontal myoseptum and inferior ventral myotomal border. Neighboring axons within the same fish served as internal controls. For these *in vivo* optogenetic axon guidance experiments, the change in axon length, growth speed, and angle of growth trajectory deviation were measured as above. In this case, an angle of 0° reflected no change in trajectory, while positive angles represent deflections in the rostral direction and negative angles represent deflections in the caudal direction. Additionally, the distance between the CaP growth cone tip and the horizontal somitic boundary was measured using FIJI (ImageJ). These distances were arbitrarily assigned positive values if the axon had not crossed the boundary and negative values if the axon had crossed into the neighboring somite. The number of axons that responded to stimulation, crossed a horizontal somitic boundary or did not respond to stimulation was counted. In one fish, the initial axon lengths could not be determined, and this fish was excluded from subsequent analysis. Since somitic units develop asynchronously in a rostral-to-caudal gradient, we treated rostral and caudal neighbors separately. Furthermore, since neighboring axons reside in the same organism, and are thus not independent observations, we fit these data with a mixed linear model that included a random effect corresponding to the animal in which axonal measurements were made. Pairwise comparisons of the least square means were performed, and p-values were adjusted for multiple comparisons using the Benjamini-Hochberg procedure for controlling the false discovery rate.

For *plod3*$^{-/-}$ rescue experiments, candidate fish were screened based the axonal guidance defect phenotype in which no CaP axons extended past the horizontal myoseptum (Figures 4,5). To quantify these experiments, the shortest distance from the horizontal myoseptum to the leading tip of the CaP axon was measured using FIJI (ImageJ)(Figure 4D). A linear model analysis was similarly applied to measurements of the distance from the tip of the CaP axon to the horizontal myoseptum in *plod3*$^{-/-}$ mutant fish, *plod3*$^{+/-}$ wildtype fish, and *plod3*$^{-/-}$ mutant fish that had been rescued with optogenetic PA-Rac1 activation. The linear model included a random variable accounting for the fish in which the measurements were made. Measurements were made on rescued axons and their neighbors in the same fish and on axons from separate *plod3*$^{+/-}$ fish identified phenotypically. Comparisons were performed as above.

Analysis of immunohistochemistry—To quantify immunohistochemical colocalization of pre- and postsynaptic proteins (SV2 and α-BT), 3D regions of interest were extracted from Z-stacks and Pearson's correlation coefficients between the SV2 and α-BT were calculated from the raw data (Figures 3E and 5C). These correlation coefficients were compared to a random distribution of correlations calculated by randomly shuffling blocks of the original images. Empiric p-values were obtained using the FIJI (ImageJ) Coloc 2 package in accordance with the Costes method (Costes, et al., 2004).

ReaChR stimulation analysis—To analyze motion from muscle contraction after ReaChR channelrhodopsin stimulation, particle image velocimetry using optical flow (PIV) analysis was performed using Fiji (ImageJ)(Figure 5E). Specifically, 2D vector fields representing the translation of 32x32 pixel boxes were generated by comparing the bright field image immediately before the initiation of contraction and the subsequent frame in which motion was first detected. These vector fields representing the motion of the zebrafish body were calculated for every observed contraction. From these vector fields, foci of contraction were localized at the site where vector fields converged. Once these foci were identified, anatomical boundaries traced from the bright field images were superimposed on the vector fields. This allowed us to determine whether the focus of contraction was in the ventral or dorsal musculature and in which somite the contraction originated. The total number of stimulations that induced any muscle contraction and the number of stimulations that induced muscle contractions specifically in the ventral musculature of the somite targeted with optogenetic stimulation were counted for the following conditions: rescued axons receiving ReaChR stimulation, rescued axons not receiving ReaChR stimulation, and neighboring unrescued axons receiving ReaChR stimulation. These data were modeled using a Poisson general linear model and p-values were computed from pairwise comparisons of the estimated marginal means (Figure 5F). Error bars represent 95% normal confidence intervals. Details of summary statistics can be found in the main text and statistical tests performed can be found in figure legends. All statistical analyses were performed in Rstudio 3.5.1 using the following packages: dplyr 0.7.6, reshape2 1.4.3, ggplot2 3.0.0, ggbeeswarm 0.6.0, lmerTest 3.0.1, gmodels 2.18.1, stats 3.5.1, lubridate 1.7.4, multcomp 1.4-10 and emmeans 1.4.2. Figures were prepared using Adobe Illustrator and BioRender.

Supplementary Material

Refer to Web version on PubMed Central for supplementary material.

Acknowledgments:

We would like to thank Juliana Brown, John Sherwood, and members of the Arlotta lab for insightful discussions and editing of the manuscript. We are grateful to Isaac Adatto and members of the Zon lab for assistance with zebrafish methodology and husbandry; Richard Schalek, Adi Suissa-Peleg, and Mariela Petkova for assistance with electron microscopy cutting, alignment, and staining procedures, respectively; and Doug Richardson and the Harvard Center for Biological Imaging staff for assistance with microscopy. We are grateful to Susan Dymecki, Roberto Chiarle, John Rinn and Raul Mostoslavsky for insightful discussions as members of JH's dissertation advisory committee. JH acknowledges support from the Harvard Stem Cell Institute MD/PhD Training Fellowship, the National Institute of Neurological Disorders and Stroke (F30 NS095520-02), the National Institute of General Medical Sciences (T32GM007753) and the HCBI Simmons Award. PA acknowledges support from the National Institute of Health (P50MH094271 and U01MH115727) and The Harvard Stem Cell Institute.

References

Airan RD, Thompson KR, Fenno LE, Bernstein H, and Deisseroth K (2009). Temporally precise in vivo control of intracellular signalling. Nature 458, 1025. [PubMed: 19295515]

Andersen SS (2001). Preparation of dissociated zebrafish spinal neuron cultures. Methods Cell Sci. 23, 205–9. [PubMed: 12486331]

Avants BW, Murphy DB, Dapello JA, and Robinson JT (2015). NeuroPG: open source software for optical pattern generation and data acquisition. Front. Neuroeng 8, 1. [PubMed: 25784873]

Beattie CE (2000). Control of motor axon guidance in the zebrafish embryo. Brain Res. Bull 53, 489–500. [PubMed: 11165784]

Berger DR, Seung HS, and Lichtman JW (2018). VAST (Volume Annotation and Segmentation Tool): Efficient Manual and Semi-Automatic Labeling of Large 3D Image Stacks. Front. Neural Circuits 12, 88. [PubMed: 30386216]

Bernhardt RR, Goerlinger S, Roos M, and Schachner M (1998). Anterior-posterior subdivision of the somite in embryonic zebrafish: implications for motor axon guidance. Dev. Dyn 213, 334–47. [PubMed: 9825868]

Boyden ES, Zhang F, Bamberg E, Nagel G, and Deisseroth K (2005). Millisecond-timescale, genetically targeted optical control of neural activity. Nat. Neurosci 8, 1263–8. [PubMed: 16116447]

Brinks D, Adam Y, Kheifets S, and Cohen AE (2016). Painting with Rainbows: Patterning Light in Space, Time, and Wavelength for Multiphoton Optogenetic Sensing and Control. Acc. Chem. Res 49, 2518–2526. [PubMed: 27786461]

Costes SV, Daelemans D, Cho EH, Dobbin Z, Pavlakis G, and Lockett S (2004). Automatic and quantitative measurement of protein-protein colocalization in live cells. Biophys. J 86, 3993–4003. [PubMed: 15189895]

David S, and Aguayo AJ (1981). Axonal elongation into peripheral nervous system "bridges" after central nervous system injury in adult rats. Science 214, 931–3. [PubMed: 6171034]

de Beco S, Vaidziulyte K, Manzi J, Dalier F, di Federico F, Cornilleau G, Dahan M, and Coppey M (2018). Optogenetic dissection of Rac1 and Cdc42 gradient shaping. Nat. Commun 9, 4816. [PubMed: 30446664]

De Marco Garcia NV, Karayannis T, and Fishell G (2011). Neuronal activity is required for the development of specific cortical interneuron subtypes. Nature 472, 351–5. [PubMed: 21460837]

Dehorter N, Ciceri G, Bartolini G, Lim L, del Pino I, and Marin O (2015). Tuning of fast-spiking interneuron properties by an activity-dependent transcriptional switch. Science 349, 1216–20. [PubMed: 26359400]

Dickson BJ (2002). Molecular mechanisms of axon guidance. Science 298, 1959–64. [PubMed: 12471249]

Eisen JS, Myers PZ, and Westerfield M (1986). Pathway selection by growth cones of identified motoneurones in live zebra fish embryos. Nature 320, 269–71. [PubMed: 3960108]

Endo M, Hattori M, Toriyabe H, Ohno H, Kamiguchi H, Iino Y, and Ozawa T (2016). Optogenetic activation of axon guidance receptors controls direction of neurite outgrowth. Sci. Rep 6, 23976. [PubMed: 27052670]

Granato M, van Eeden FJ, Schach U, Trowe T, Brand M, Furutani-Seiki M, Haffter P, Hammerschmidt M, Heisenberg CP, Jiang YJ, et al. (1996). Genes controlling and mediating locomotion behavior of the zebrafish embryo and larva. Development 123, 399–413. [PubMed: 9007258]

Haase G, Dessaud E, Garcès A, de Bovis B, Birling M-C, Filippi P, Schmalbruch H, Arber S, and deLapeyrière O (2002). GDNF Acts through PEA3 to Regulate Cell Body Positioning and Muscle Innervation of Specific Motor Neuron Pools. Neuron 35, 893–905. [PubMed: 12372284]

Hakim R, Shamardani K, and Adesnik H (2018). A neural circuit for gamma-band coherence across the retinotopic map in mouse visual cortex. Elife 7.

Hall A, and Lalli G (2010). Rho and Ras GTPases in axon growth, guidance, and branching. Cold Spring Harb. Perspect. Biol 2, a001818. [PubMed: 20182621]

Hayashi-Takagi A, Yagishita S, Nakamura M, Shirai F, Wu YI, Loshbaugh AL, Kuhlman B, Hahn KM, and Kasai H (2015). Labelling and optical erasure of synaptic memory traces in the motor cortex. Nature 525, 333–8. [PubMed: 26352471]

Hayworth KJ, Morgan JL, Schalek R, Berger DR, Hildebrand DG, and Lichtman JW (2014). Imaging ATUM ultrathin section libraries with WaferMapper: a multi-scale approach to EM reconstruction of neural circuits. Front. Neural Circuits 8, 68. [PubMed: 25018701]

Hilario JD, Rodino-Klapac LR, Wang C, and Beattie CE (2009). Semaphorin 5A is a bifunctional axon guidance cue for axial motoneurons *in vivo*. Dev. Biol 326, 190–200. [PubMed: 19059233]

Hildebrand DGC, Cicconet M, Torres RM, Choi W, Quan TM, Moon J, Wetzel AW, Scott Champion A, Graham BJ, Randlett O, et al. (2017). Whole-brain serial-section electron microscopy in larval zebrafish. Nature 545, 345–349. [PubMed: 28489821]

Hua Y, Laserstein P, and Helmstaedter M (2015a). Large-volume en-bloc staining for electron microscopy-based connectomics. Nat. Commun. 6, 7923. [PubMed: 26235643]

Hua ZL, Emiliani FE, and Nathans J (2015b). Rac1 plays an essential role in axon growth and guidance and in neuronal survival in the central and peripheral nervous systems. Neural Dev. 10, 21. [PubMed: 26395878]

Jacobs CL, Badiee RK, and Lin MZ (2018). StaPLs: versatile genetically encoded modules for engineering drug-inducible proteins. Nat. Methods 15, 523–526. [PubMed: 29967496]

Joesch M, Mankus D, Yamagata M, Shahbazi A, Schalek R, Suissa-Peleg A, Meister M, Lichtman JW, Scheirer WJ, and Sanes JR (2016). Reconstruction of genetically identified neurons imaged by serial-section electron microscopy. Elife 5.

Jung H, Kang H, and Nam Y (2017). Digital micromirror based near-infrared illumination system for plasmonic photothermal neuromodulation. Biomed. Opt. Express 8, 2866–2878. [PubMed: 28663912]

Kawakami K, and Shima A (1999). Identification of the Tol2 transposase of the medaka fish Oryzias latipes that catalyzes excision of a nonautonomous Tol2 element in zebrafish Danio rerio. Gene 240, 239–44. [PubMed: 10564832]

Kim J-M, Hwa J, Garriga P, Reeves PJ, RajBhandary UL, and Khorana HG (2005). Light-Driven Activation of β2-Adrenergic Receptor Signaling by a Chimeric Rhodopsin Containing the β2-Adrenergic Receptor Cytoplasmic Loops. Biochemistry 44, 2284–2292. [PubMed: 15709741]

Kou SY, Chiu AY, and Patterson PH (1995). Differential regulation of motor neuron survival and choline acetyltransferase expression following axotomy. J. Neurobiol 27, 561–72. [PubMed: 7561834]

Kwan KM, Fujimoto E, Grabher C, Mangum BD, Hardy ME, Campbell DS, Parant JM, Yost HJ, Kanki JP, and Chien CB (2007). The Tol2kit: a multisite gateway-based construction kit for Tol2 transposon transgenesis constructs. Dev. Dyn 236, 3088–99. [PubMed: 17937395]

Lin JH, Saito T, Anderson DJ, Lance-Jones C, Jessell TM, and Arber S (1998). Functionally Related Motor Neuron Pool and Muscle Sensory Afferent Subtypes Defined by Coordinate ETS Gene Expression. Cell 95, 393–407. [PubMed: 9814709]

Lin JY, Knutsen PM, Muller A, Kleinfeld D, and Tsien RY (2013). ReaChR: a red-shifted variant of channelrhodopsin enables deep transcranial optogenetic excitation. Nat. Neurosci 16, 1499–508. [PubMed: 23995068]

Lohof AM, Quillan M, Dan Y, and Poo MM (1992). Asymmetric modulation of cytosolic cAMP activity induces growth cone turning. J. Neurosci 12, 1253–61. [PubMed: 1372932]

Lungu OI, Hallett RA, Choi EJ, Aiken MJ, Hahn KM, and Kuhlman B (2012). Designing photoswitchable peptides using the AsLOV2 domain. Chem. Biol 19, 507–17. [PubMed: 22520757]

Melancon E, Liu DW, Westerfield M, and Eisen JS (1997). Pathfinding by identified zebrafish motoneurons in the absence of muscle pioneers. J. Neurosci 17, 7796–804. [PubMed: 9315900]

Myers PZ, Eisen JS, and Westerfield M (1986). Development and axonal outgrowth of identified motoneurons in the zebrafish. J. Neurosci 6, 2278–89. [PubMed: 3746410]

Nagel G, Brauner M, Liewald JF, Adeishvili N, Bamberg E, and Gottschalk A (2005). Light Activation of Channelrhodopsin-2 in Excitable cells of Caenorhabditis elegans triggers rapid behavioral responses. Curr. Biol 15, 2279–2284. [PubMed: 16360690]

Ng J, Nardine T, Harms M, Tzu J, Goldstein A, Sun Y, Dietzl G, Dickson BJ, and Luo L (2002). Rac GTPases control axon growth, guidance and branching. Nature 416, 442–7. [PubMed: 11919635]

Pallas SL, Littman T, and Moore DR (1999). Cross-modal reorganization of callosal connectivity without altering thalamocortical projections. Proc. Natl. Acad. Sci. U. S. A 96, 8751–6. [PubMed: 10411947]

Pallas SL, Roe AW, and Sur M (1990). Visual projections induced into the auditory pathway of ferrets. I. Novel inputs to primary auditory cortex (AI) from the LP/pulvinar complex and the topography of the MGN-AI projection. J. Comp. Neurol 298, 50–68. [PubMed: 1698829]

Pallas SL, and Sur M (1993). Visual projections induced into the auditory pathway of ferrets: II. Corticocortical connections of primary auditory cortex. J. Comp. Neurol 337, 317–33. [PubMed: 8277005]

Panzer JA, Gibbs SM, Dosch R, Wagner D, Mullins MC, Granato M, and Balice-Gordon RJ (2005). Neuromuscular synaptogenesis in wild-type and mutant zebrafish. Dev. Biol 285, 340–57. [PubMed: 16102744]

Pasterkamp RJ, Giger RJ, Ruitenberg MJ, Holtmaat AJ, De Wit J, De Winter F, and Verhaagen J (1999). Expression of the gene encoding the chemorepellent semaphorin III is induced in the fibroblast component of neural scar tissue formed following injuries of adult but not neonatal CNS. Mol. Cell. Neurosci 13, 143–66. [PubMed: 10192772]

Piantino J, Burdick JA, Goldberg D, Langer R, and Benowitz LI (2006). An injectable, biodegradable hydrogel for trophic factor delivery enhances axonal rewiring and improves performance after spinal cord injury. Exp. Neurol 201, 359–67. [PubMed: 16764857]

Quadrato G, and Arlotta P (2017). Present and future of modeling human brain development in 3D organoids. Curr. Opin. Cell Biol 49, 47–52. [PubMed: 29227864]

Richardson PM, McGuinness UM, and Aguayo AJ (1980). Axons from CNS neurons regenerate into PNS grafts. Nature 284, 264–5. [PubMed: 7360259]

Roos M, Schachner M, and Bernhardt RR (1999). Zebrafish semaphorin Z1b inhibits growing motor axons in vivo. Mech. Dev 87, 103–17. [PubMed: 10495275]

Rosowski EE, Deng Q, Keller NP, and Huttenlocher A (2016). Rac2 Functions in Both Neutrophils and Macrophages To Mediate Motility and Host Defense in Larval Zebrafish. J. Immunol 197, 4780–4790. [PubMed: 27837107]

Russ JB, and Kaltschmidt JA (2014). From induction to conduction: how intrinsic transcriptional priming of extrinsic neuronal connectivity shapes neuronal identity. Open Biol. 4, 140144. [PubMed: 25297387]

Ryu M-H, Moskvin OV, Siltberg-Liberles J, and Gomelsky M (2010). Natural and engineered photoactivated nucleotidyl cyclases for optogenetic applications. J. Biol. Chem 285, 41501–41508. [PubMed: 21030591]

Sakai S, Ueno K, Ishizuka T, and Yawo H (2013). Parallel and patterned optogenetic manipulation of neurons in the brain slice using a DMD-based projector. Neurosci. Res 75, 59–64. [PubMed: 22469653]

Schneider VA, and Granato M (2006). The myotomal diwanka (lh3) glycosyltransferase and type XVIII collagen are critical for motor growth cone migration. Neuron 50, 683–95. [PubMed: 16731508]

Schnell L, Schneider R, Kolbeck R, Barde YA, and Schwab ME (1994). Neurotrophin-3 enhances sprouting of corticospinal tract during development and after adult spinal cord lesion. Nature 367, 170–3. [PubMed: 8114912]

Siebert JR, Conta Steencken A, and Osterhout DJ (2014). Chondroitin sulfate proteoglycans in the nervous system: inhibitors to repair. Biomed. Res. Int 2014, 845323. [PubMed: 25309928]

Sur M, Angelucci A, and Sharma J (1999). Rewiring cortex: the role of patterned activity in development and plasticity of neocortical circuits. J. Neurobiol 41, 33–43. [PubMed: 10504190]

Tamplin OJ, Cox BJ, and Rossant J (2011). Integrated microarray and ChIP analysis identifies multiple Foxa2 dependent target genes in the notochord. Dev. Biol 360, 415–25. [PubMed: 22008794]

Tapia JC, Kasthuri N, Hayworth KJ, Schalek R, Lichtman JW, Smith SJ, and Buchanan J (2012). High-contrast en bloc staining of neuronal tissue for field emission scanning electron microscopy. Nat. Protoc 7, 193–206. [PubMed: 22240582]

Tessier-Lavigne M (2002). Wiring the brain: the logic and molecular mechanisms of axon guidance and regeneration. Harvey Lect. 98, 103–43. [PubMed: 16033159]

Tessier-Lavigne M, and Goodman CS (1996). The molecular biology of axon guidance. Science 274, 1123–33. [PubMed: 8895455]

Velasco S, Kedaigle AJ, Simmons SK, Nash A, Rocha M, Quadrato G, Paulsen B, Nguyen L, Adiconis X, Regev A, et al. (2019). Individual brain organoids reproducibly form cell diversity of the human cerebral cortex. Nature 570, 523–527. [PubMed: 31168097]

Walter J, Kern-Veits B, Huf J, Stolze B, and Bonhoeffer F (1987). Recognition of position-specific properties of tectal cell membranes by retinal axons *in vitro*. Development 101, 685–96. [PubMed: 3503693]

Wheeler BC, and Brewer GJ (2010). Designing Neural Networks in Culture: Experiments are described for controlled growth, of nerve cells taken from rats, in predesigned geometrical patterns on laboratory culture dishes. Proc. IEEE Inst. Electr. Electron. Eng 98, 398–406. [PubMed: 21625406]

White RM, Sessa A, Burke C, Bowman T, LeBlanc J, Ceol C, Bourque C, Dovey M, Goessling W, Burns CE, et al. (2008). Transparent adult zebrafish as a tool for in vivo transplantation analysis. Cell Stem Cell 2, 183–9. [PubMed: 18371439]

Wu YI, Frey D, Lungu OI, Jaehrig A, Schlichting I, Kuhlman B, and Hahn KM (2009). A genetically encoded photoactivatable Rac controls the motility of living cells. Nature 461, 104–8. [PubMed: 19693014]

Yazawa M, Sadaghiani AM, Hsueh B, and Dolmetsch RE (2009). Induction of protein-protein interactions in live cells using light. Nat. Biotechnol 27, 941. [PubMed: 19801976]

Yiu G, and He Z (2006). Glial inhibition of CNS axon regeneration. Nat. Rev. Neurosci 7, 617–27. [PubMed: 16858390]

Yoo SK, Deng Q, Cavnar PJ, Wu YI, Hahn KM, and Huttenlocher A (2010). Differential Regulation of Protrusion and Polarity by PI(3)K during Neutrophil Motility in Live Zebrafish. Dev. Cell 18, 226–236. [PubMed: 20159593]

Zelenchuk TA, and Bruses JL (2011). In vivo labeling of zebrafish motor neurons using an mnx1 enhancer and Gal4/UAS. Genesis 49, 546–54. [PubMed: 21538811]

Zeller J, and Granato M (1999). The zebrafish diwanka gene controls an early step of motor growth cone migration. Development 126, 3461–72. [PubMed: 10393124]

Zhao S, Cunha C, Zhang F, Liu Q, Gloss B, Deisseroth K, Augustine GJ, and Feng G (2008). Improved expression of halorhodopsin for light-induced silencing of neuronal activity. Brain Cell Biol. 36, 141–154. [PubMed: 18931914]

Highlights

- Axonal growth trajectories are controlled with light by optogenetic Rac1 activation
- Endogenous axon guidance programs are overridden to create novel circuitry *in vivo*
- Defective axonal architecture is repaired, restoring long-range axonal connectivity
- Functional synaptic connections are created following optogenetic axon guidance

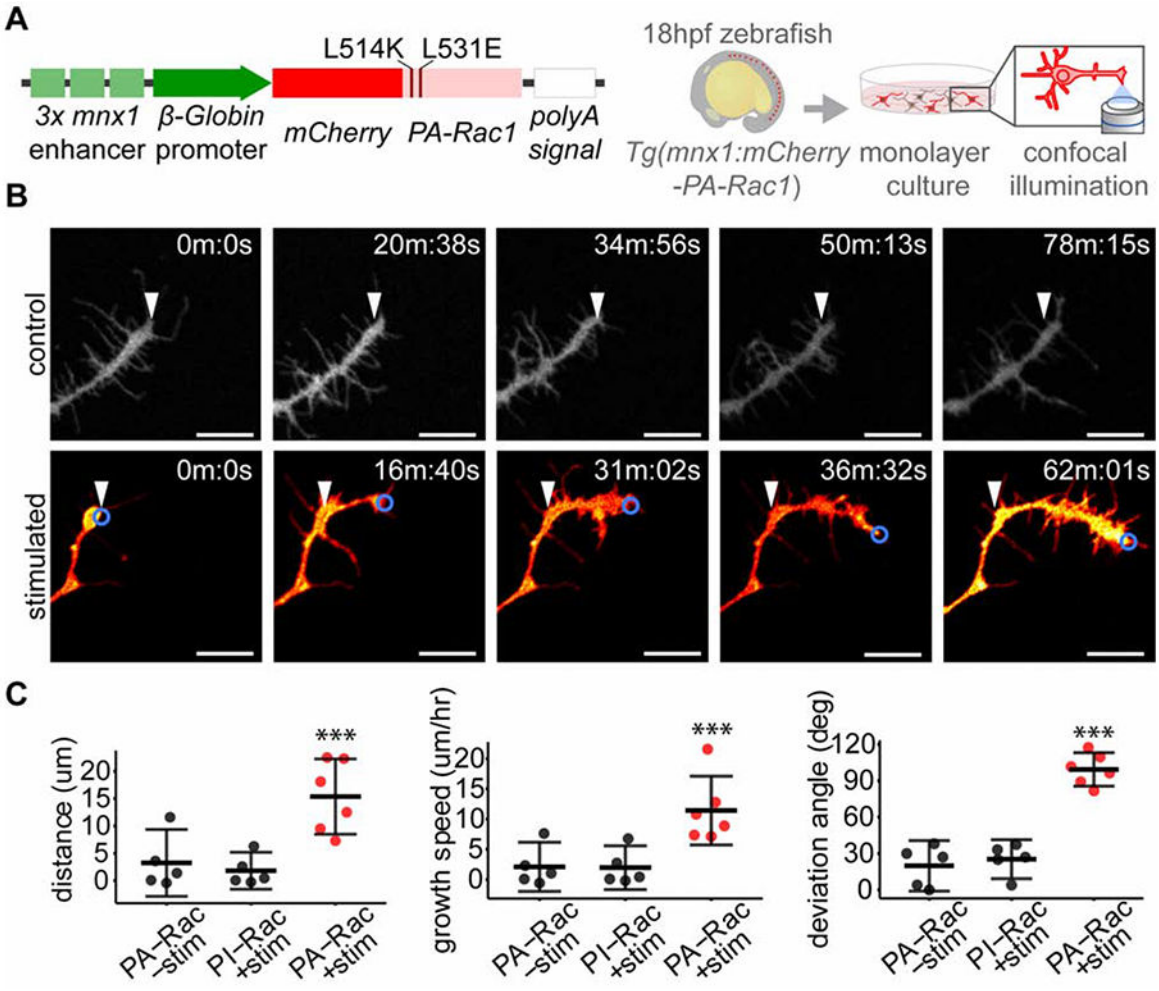

Figure 1. Optogenetic stimulation of PA-Rac1 resulted in directed axonal growth of cultured zebrafish spinal motor neuron axons.

(A) Schematic of expression construct and experimental design. **(B)** Time series of cultured PA-Rac1^{+} neurons, either unstimulated (top row) or illuminated in a region of interest focused on the leading edge of the growth cone (blue circle) (bottom row). White arrowheads indicate the initial position of the growth cone (scale bar 10μm). **(C)** Stimulated axons (n=5 axons from separate cultures of independent embryos) grew significantly greater distances over the trial period (left), resulting in a faster rate of growth (middle), and deviated significantly from their initial trajectory compared to unilluminated PA-Rac1^{+} axons or illuminated photo-insensitive Rac1^{+} (PI-Rac1) axons (right, independent samples Student's T-test, **p<0.01, *** p<0.001. Mean and 95% confidence intervals shown). See also Figure S1, Movie S1.

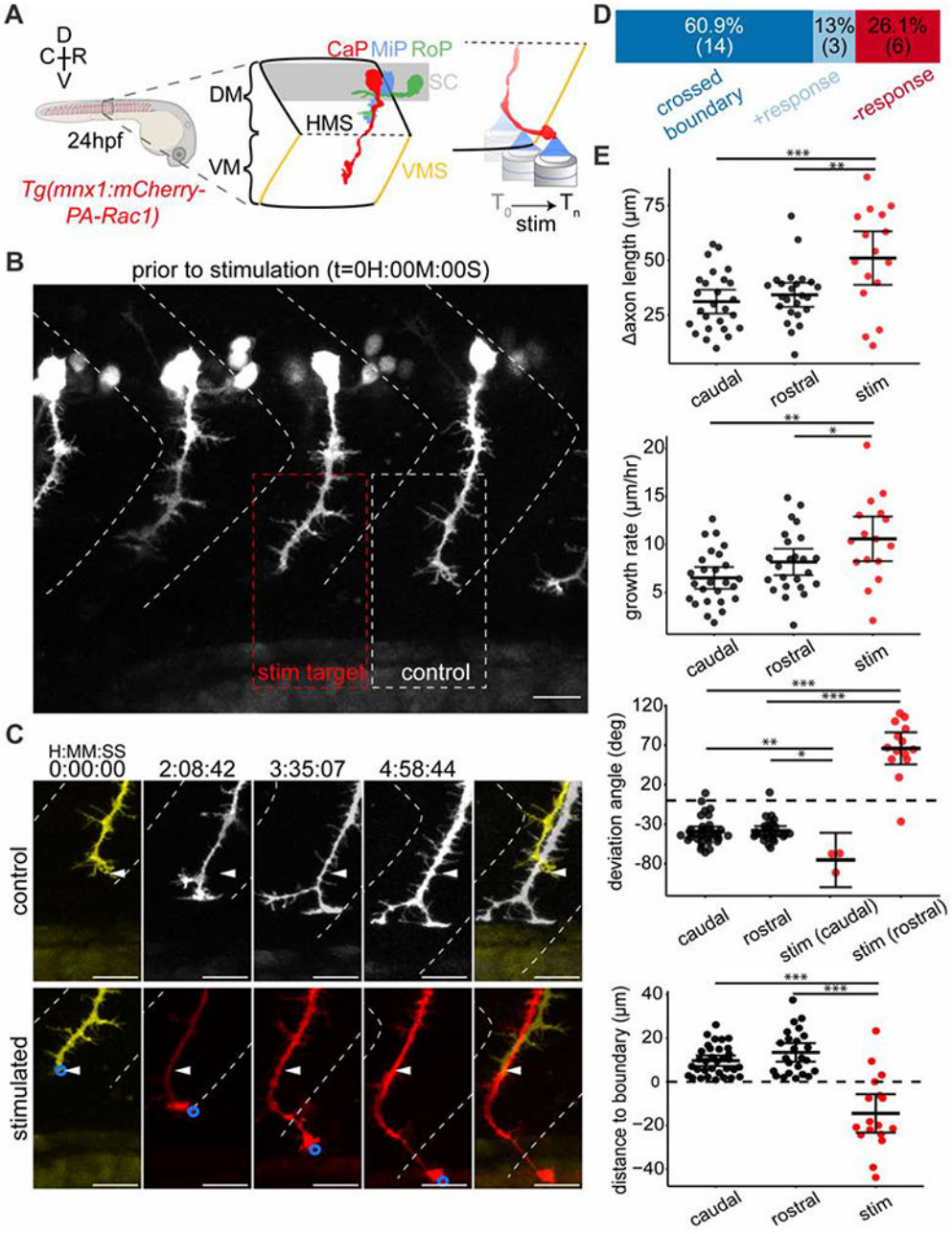

Figure 2. Optogenetic stimulation of PA-Rac1 directed zebrafish CaP axon growth across the repulsive somitic boundary into the neighboring somitic musculature.

(A) Schematic of experimental design: zebrafish expressing PA-Rac1 in CaP neurons (left) were illuminated at the leading edge of the growth cone from 24 to 29hpf (right) **(B)** Position of axons prior to stimulation. All CaP neurons were within the somitic boundaries (dashed white chevrons). A single CaP axonal growth cone per fish (red box) was asymmetrically illuminated, while other CaP neurons, including the rostral neighbor (white box), remained unilluminated (scale bar 20μm). **(C)** Time series of CaP axons in an unstimulated rostral axon (upper series, corresponding to white dashed box in (B)) and illuminated CaP axon (lower series, corresponding to red box in (B)). The stimulated axon

was guided across the rostral somitic boundary, while the unstimulated axon remained entirely within its native somite (arrowheads indicate the initial position of the axon; scale bar 20μm). **(D)** Distribution of outcomes of optogenetic stimulation. **(E)** PA-Rac1-mediated guidance of CaP axons *in vivo* resulted in significantly longer axons over the trial period, corresponding to faster axonal growth (top two graphs respectively, n=16 axons, one axon per zebrafish). The angle of axon growth deviated significantly in both the rostral and caudal directions from their initial trajectory compared with unilluminated controls (middle). Stimulated axons were guided across the somitic boundary, which control axons never crossed [bottom, negative values indicate growth across the somitic boundary, (FDR adjusted, difference of least square means from mixed linear model, n=17 axons, one axon per fish, * $p<0.05$, ** $p<0.01$, *** $p<0.001$), mean and 95% confidence intervals shown]. R-Rostral; C-Caudal; D-Dorsal; V-Ventral; DM-dorsal myotome; SC-spinal cord; VM-ventral myotome; HMS-horizontal myoseptum; VMS-vertical myoseptum; CaP, MiP, and RoP-caudal, middle and rostral primary spinal motor neurons, respectively. See also Figure S1, Movie S2.

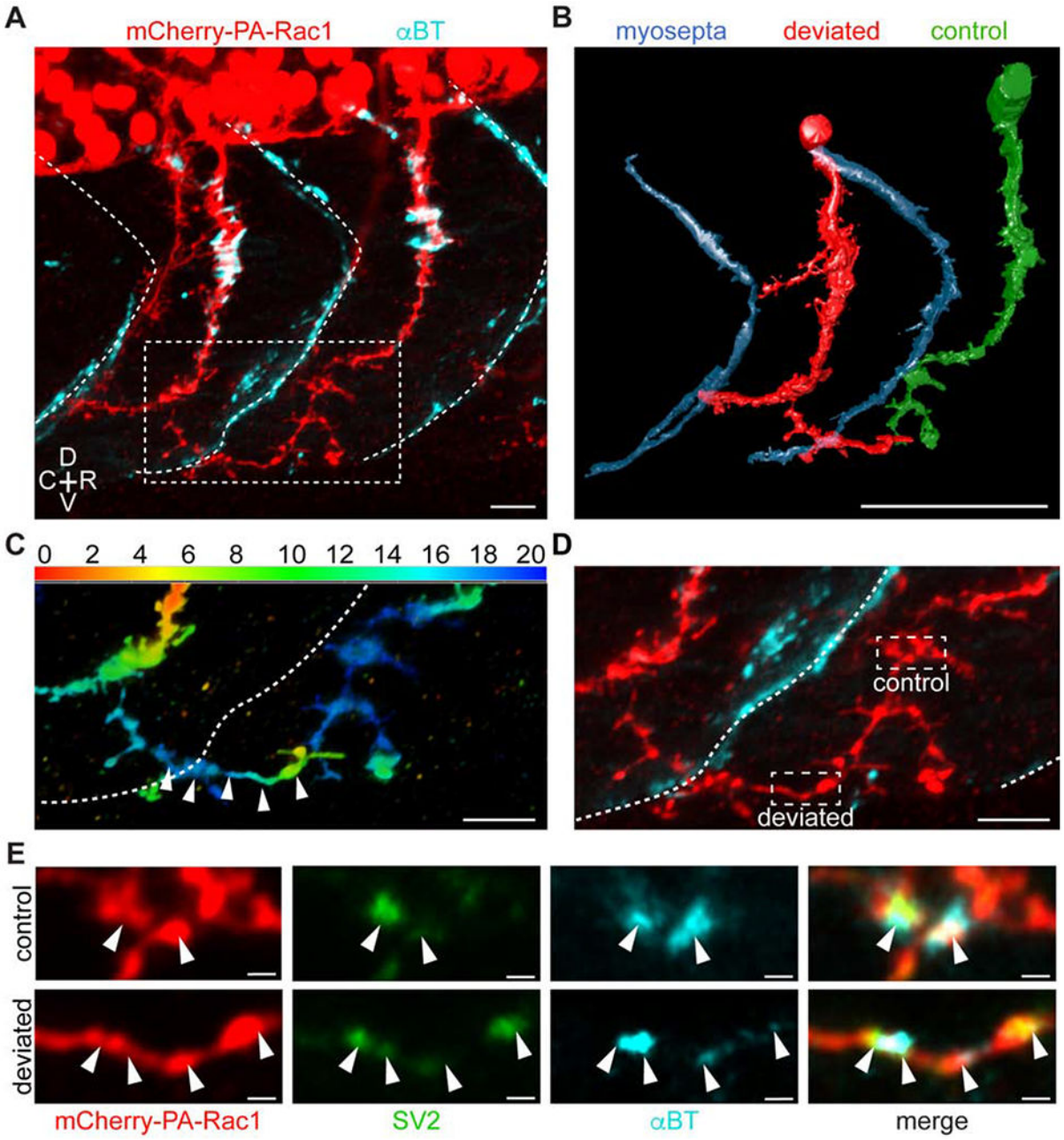

Figure 3. Molecular investigation of novel neuromuscular synaptic formation between ectopically-directed CaP neuron and foreign myotomes

(A) Z-projection of a zebrafish CaP neuron (red) deviated across a somitic boundary (dashed white line), revealed by a-bungarotoxin staining (cyan; scale bar 10μm). **(B)** A 3D rendering from confocal stacks of the deviated (red) and neighboring control (green) axon in (A) with the somitic boundary (blue; scale bar 50μm) (see also Movie S3). **(C)** The axonal segments in the white dashed box in (A), pseudocolored to reflect Z-position of the deviated CaP axon (white arrowheads), which passed lateral to the neighboring rostral CaP neuron (scale bar 10μm). **(D)** Same region as (C), showing the locations of the regions of interest in E on the unstimulated CaP axon (dashed white box, control) and the invading CaP axon (dashed

white box, deviated; scale bar 10μm). **(E)** Immunohistochemistry of regions of interest in (D) for mCherry-PA-Rac1 (red), synaptic vesicle 2 (SV2, green), and α-bungarotoxin (αBT, cyan) for the unstimulated control axon (top) and stimulated axon deviated across the somitic boundary (bottom). White arrowheads illustrate the colocalization of pre- and post-synaptic markers, suggesting the presence of synapses (n=3 fish, Costes p-value>0.95; scale bar 1 μm). R- rostral, C-caudal, D-dorsal, V-ventral. See also Figure S2, Movie S3.

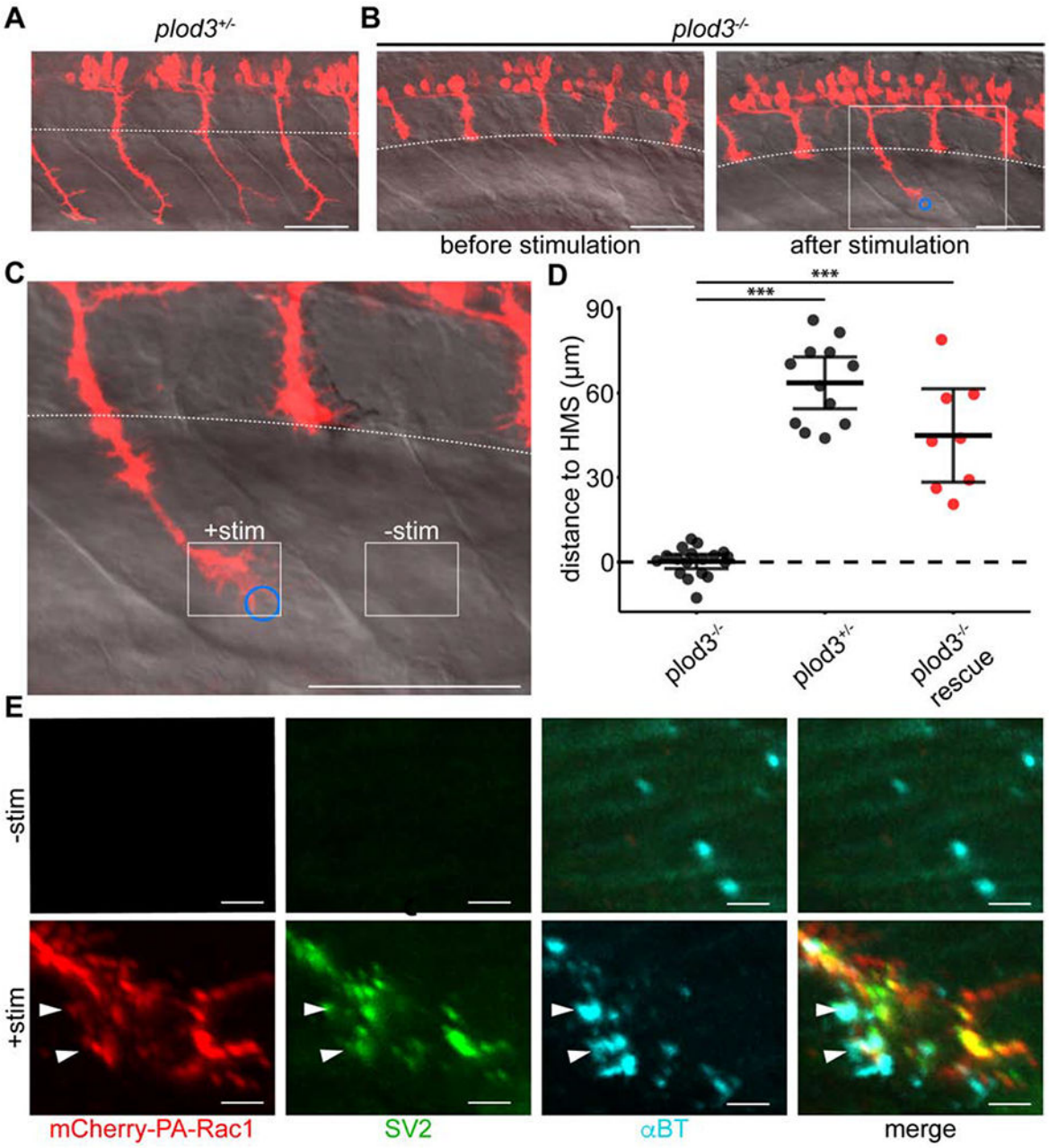

Figure 4. Optogenetic stimulation of *plod3*$^{-/-}$ zebrafish CaP neurons rescues their axon guidance defect, allowing juxtaposition of pre- and postsynaptic machinery within the ventral myotome.

(A) PA-Rac1 expression (red) in spinal motor neurons of *plod3*$^{+/-}$ zebrafish at 28hpf (scale bar 50µm). **(B)** Left: An age-matched *plod3*$^{-/-}$ mutant sibling prior to stimulation fails to extend CaP axons into the ventral myotome past the horizontal myoseptum (dashed white line). Right: In *plod3*$^{-/-}$ fish, a single PA-Rac1^{+} CaP axon extended into the ventral myotome after illumination, while unilluminated axons remain arrested at the horizontal myoseptum. (blue circle: region of illumination; scale bar 50µm). **(C)** Enlarged image of *plod3*$^{-/-}$ CaP axon following stimulation (solid white box in (B); scale bar 50 µm). **(D)** Illumination of PA-Rac1^{+} CaP axons in *plod3*$^{-/-}$ mutant fish induced growth significantly

farther past the horizontal myoseptum than unilluminated axons. There was no significant difference in the distance grown past the horizontal myoseptum in illuminated *plod3*$^{-/-}$ fish compared to *plod*$^{+/-}$ fish (FDR adjusted, difference of least square means from mixed linear model, n=8 axons, one axon per fish, *** $p<0.001$, mean and 95% confidence intervals shown). **(E)** Immunohistochemistry for mCherry (red, left), SV2 (green, middle left), and αBT (cyan, middle right) showing colocalization of pre- and post-synaptic markers (merge, right) in the ventral myotome of the stimulated axon (bottom), but not in the unstimulated axon (top; scale bar 5μm). Stimulated and unstimulated regions correspond to solid white boxes in (C). See also Movie S4.

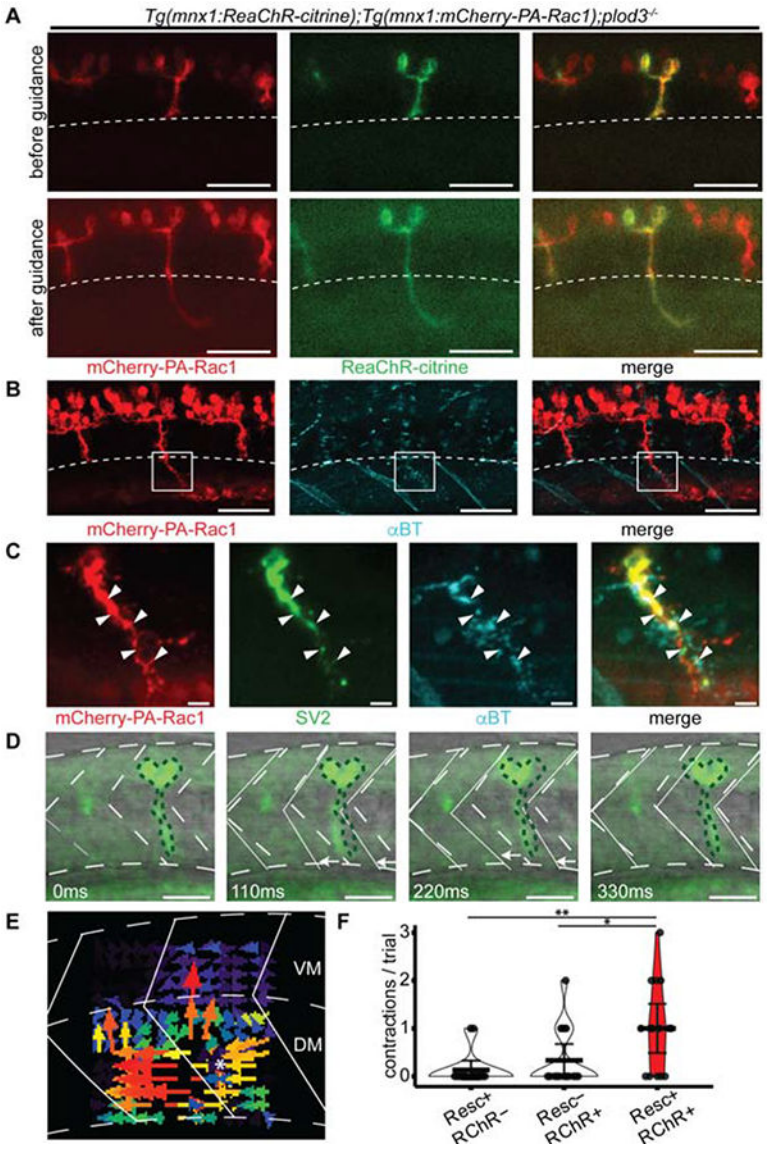

Figure 5. Functional restoration of synaptic connectivity with ventral myotome following rescue of *plod3*$^{-/-}$ zebrafish CaP axons.

(A) Before (top) and after (bottom) PA-Rac1 optogenetic-mediated rescue of *plod3*$^{-/-}$ mutant zebrafish expressing both mCherry-PA-Rac1 (red, left) and ReaChR-citrine (green, middle) transgenes (merge right, scale bar 50μm). Only the rescued axon extends into the dorsal myotome, past the horizontal myoseptum (dashed white line) See also Movie S5. **(B)** Immunohistochemistry for mCherry (red, left) and αBT (cyan, middle) illustrates that only the rescued axon extends past the horizontal myoseptum (merge, right; scale bar 50μm). Note that red-channel fluorescence ventral to the indicated ROI is from nonspecific accumulation of secondary antibody in the yolk sac. **(C)** Immunohistochemistry for mCherry (red, left), SV2 (green, middle left), and αBT (cyan, middle right), showed significant colocalization of pre- and post-synaptic markers (merge, right; n=3 fish, Costes p-value>0.95) in the ventral myotome of the stimulated axon (solid white box in B; scale bar 5μm). **(D)** Time series of ventral myofibril contractions following ReaChR stimulation of a

rescued CaP axon. The dotted green lines show the initial position of the axon. The white arrows show the movement of the somatic boundaries (white lines) in the ventral, but not dorsal, myotome compared with time 0 (grey dashed lines; scale bar 50μm) **(E)** Vector fields representing the motion of the zebrafish body wall following ReaChR stimulation of a rescued CaP axon, computed via particle image velocimetry using optical flow analysis of bright field time series images. Color-coded arrows represent the direction and magnitude of optical flow; the point of vector field convergence that indicates the initial focus of contraction is marked by a white asterisk. For the majority of elicited motor responses, the contraction occurred specifically in the somite innervated by the rescued axon (15/17 contractions, see also Movies S6,7). **(F)** Optogenetic depolarization of rescued *plod3*$^{-/-}$ axons via activation of ReaChR channelrhodopsin (Resc^{+} RChR^{+}) resulted in significantly more contractions of ventral myofibrils in the targeted somite compared with ReaChR activation of a neighboring axon that had not been rescued (Resc^{-} RChR^{+}) or illumination of the rescued axon stimulated with wavelengths of light outside of the ReaChR activation spectrum (Resc^{+} RChR^{-}). (Pairwise comparison of estimated marginal means from a Poisson general linear model, n=3 fish, 5 trials per condition, * $p<0.05$, ** $p<0.01$. mean and 95% confidence intervals shown; see also Movie S6).

KEY RESOURCES TABLE

REAGENT or RESOURCE	SOURCE	IDENTIFIER
Antibodies		
Mouse monoclonal anti-synaptic vesicle 2 (Clone SV2)	DSHB	Cat#SV2; RRID: AB_2315387
Rabbit polyclonal anti-RFP	Rockland	Cat#600-401-379S Lot 35868; RRID: AB_2209751
Rabbit polyclonal anti-Thr423 phospho-PAK1	Cell Signaling Technology	Cat#2601T; RRID: AB_330220
Rat monoclonal anti-RFP (Clone 5F8)	ChromoTek	Cat#5F8; RRID: AB_2336064
AlexaFluor 488 conjugated goat anti-mouse	Invitrogen	Cat#A11001; RRID: AB_2534069
AlexaFluor 488 conjugated goat anti-rabbit	Invitrogen	Cat#A11008; RRID: AB_143165
AlexaFluor 546 conjugated goat anti-rabbit	Invitrogen	Cat#A11035; RRID: AB_143051
AlexaFluor 546 conjugated got anti-rat	Invitrogen	Cat#A11081; RRID: AB_141738
Chemicals, Peptides, and Recombinant Proteins		
Leibovitz's L-15 media	Thermo Fisher	Cat#2108027
Alpha-bungarotoxin, Alexa Fluor 647 conjugate	Thermo Fisher	Cat#B35450
LR Clonase II Plus	Invitrogen	Cat#12538200
Quick T4 DNA ligase	Neb	Cat#M2200S
Poly-D-Lysine	VWR	Cat#35210
Laminin	VWR	Cat#354232
Ethyl 3-aminobenzoate (Tricaine, MS222)	Sigma-Aldrich	Cat#E10505
Agarose type II (low melting point)	Sigma-Aldrich	Cat#A6877
Trizol LS	Thermo Fisher	Cat#10296010
Collagenase	Sigma-Aldrich	Cat#C9891
Critical Commercial Assays		
DNAeasy Blood and Tissue Kit	Qiagen	69504
Custom TaqMan SNP Genotyping Assay	Thermo Fischer	Cat#4332077; AssayID: ANXGU9F
pENTR 5'-TOPO TA-Cloning Kit	Invitrogen	Cat#K59120
pENTR/D-TOPO cloning kit	Invitrogen	Cat#K240020
Q5 site directed mutagenesis kit	NEB	Cat#E0554S
Gibson Assembly kit	NEB	Cat#E5510S
NEBuilder HiFi DNA assembly kit	NEB	Cat#E2621
RNAeasy Mini Kit	Qiagen	Cat#74104
QX200 Evagreen ddPCR super mix	BioRad	Cat#1864033
iScript Select cDNA synthesis kit	BioRad	Cat#1708896
Experimental Models: Organisms/Strains		
Zebrafish: *mitfa*^{w2};*mpv17*^{a9}: w2/w2;a9/a9	Zon Lab (White et al., 2008; ZIRC.	ZIRC Cat#ZL1714; RRID: ZFIN_ZDB-GENO-080326-11
Zebrafish: *plod3*^{tv205a}: tv205a/+ and tv205a/tv205a	Granato et al., 1996, Schneider and Granato, 2006; EZRC	EZRC Cat#941; RRID: ZFIN_ZDB-GENO-980202-1211

REAGENT or RESOURCE	SOURCE	IDENTIFIER
Zebrafish: *Tg(mnx1:mCherry-PA-Rac1);mitfa^{w2};mpv17^{a9}*: Tg;w2/w2;a9/a9	This Paper	N/A
Zebrafish: *Tg(mnx1:mCherry-PI-Rac1);mitfa^{w2};mpv17^{a9}*: Tg;w2/w2;a9/a9	This Paper	N/A
Zebrafish: *Tg(mnx1:mCherry-PA-Rac1);plod3^{tv205a}*: Tg;tv205a/tv205a and Tg;tv205a/+	This Paper	N/A
Zebrafish: *Tg(mnx1:ReaChR-citrine);Tg(mnx1:mCherry-PA-Rac1);plod3^{tv205a}*: Tg;Tg;tv205a/tv205a	This Paper	N/A
Oligonucleotides		
Primers for transgenesis construct cloning (see Table S1)		
Primers for ddPCR (see Table S1)		
Recombinant DNA		
Plasmid: *pTriEx-mCherry-PA-Rac1*	Wu et al., 2009	Addgene Plasmid #22027
Plasmid: *pTriEx-mCherry-PA-Rac1-C450A*	Wu et al., 2009	Addgene Plasmid #22028
Plasmid: *pLenti-ReaChR-citrine*	Lin et al., 2013	Addgene Plasmid #50956
Plasmid: *p3E-SV40-poly-A*	Kwan et al., 2007;; http://tol2kit.genetics.utah.edu/index.php/List_of_entry_and_destination_vectors	Plasmid#302
Plasmid: *pDestTol2CG2*	Kwan et al., 2007; http://tol2kit.genetics.utah.edu/index.php/List_of_entry_and_destination_vectors	Plasmid#395
Plasmid: *pCS2FA-transposase*	Kwan et al., 2007; http://tol2kit.genetics.utah.edu/index.php/List_of_entry_and_destination_vectors	Plasmid#396
Plasmid: *p5E-3x125bp-mnx1*	Zelenchuk and Bruses, 2011; This Paper	N/A
Plasmid: *pDestTol2CG2-mnx1:mCherry-PA-Rac1*	This Paper	N/A
Plasmid: *pDestTol2CG2-mnx1:mCherry-PI-Rac1*	This Paper	N/A
Plasmid: *pDestTol2CG2-mnx1:ReaChR-citrine*	This Paper	N/A
Software and Algorithms		
Zen Black	Zeiss	https://www.zeiss.com/microscopy/us/products/microscope-software/zen.html; RRID:SCR_018163
Fiji (ImageJ)	Schneider et al., 2012	https://fiji.sc/; RRID:SCR_002285
VAST	Berger et al., 2018	https://software.rc.fas.harvard.edu/lichtman/vast/
Imaris	Bitplane	https://imaris.oxinst.com/packages; RRID:SCR_007370
Rstudio	Rstudio	https://rstudio.com/; RRID:SCR_000432
Illustrator	Adobe Studios	https://www.adobe.com/products/illustrator.html; RRID:SCR_018012
Statistical analyses and image processing scripts	This Paper	https://github.com/jharris9/optogenetic_axon_guidance_analysis
Other		

REAGENT or RESOURCE	SOURCE	IDENTIFIER
Zeiss LSM 880 Microscope with Airyscan detector	Zeiss	N/A
Zeiss LSM 880 Microscope with GaSaP detector	Zeiss	N/A
Sigma scanning electron microscope	Zeiss	N/A
7900HT RT-PCR machine	Applied Biosystems	N/A
MoFlo XDP Cell Sorter with Summit 5.4 data collection software	Beckman Coulter	ML99030
QX200 ddPCR machine	BioRad	N/A
Attafluor Cell Chambers	Thermo Fischer	Cat#A-7816